

1 **Dear Todd Ehlers,**

2

3 **Thank you very much for the review. We included the suggested revisions into the manuscript.**

4

5 *This manuscript received two thorough and thoughtful reviews that identified areas of the manuscript*
6 *where clarification was needed. Both reviewers are experts in either the field of bioturbation and*
7 *landscape modeling approaches. The primary areas where changes were requested included: a)*
8 *clarification of the 'new' aspects of the study and improved comparisons to previous work; b) more*
9 *precise presentation of results in figures and associated text; and c) improved presentation of the*
10 *modeling approach used.*

11

12 *The authors have done a thorough job addressing the reviewer's comments, and I thank them for the*
13 *detailed response to reviews and figure/table/ and text revisions. The text (and figure changes)*
14 *presented in response to reviews nicely address the reviewer's comments - and represent substantial*
15 *revisions.*

16

17 *Unfortunately, (not the author's fault) I didn't see an uploaded version of the revised manuscript text and*
18 *figures on the website. I realize the Copernicus website doesn't explicitly ask for this. However, many*
19 *authors often included the full revised manuscript (with track changes) at the end of their review*
20 *response. Given this, I kindly ask the authors to upload (after some minor suggestions I make below)*
21 *the revised version of their manuscript and figures (with track changes for the text) to the website. This*
22 *version should include the changes indicated in their response to reviews. If the authors did not track*
23 *changes during revisions, then they can (in MS Word at least) use the option to difference the revised*
24 *and original versions of the text to have a succinct summary of changes.*

25

26 **We provide the manuscript with all track changes highlighted in green below this rebuttal letter.**

27

28 *Two additional (minor) changes I ask the authors to make:*

29

30 *First, the text (and response to reviews) repeatedly says "Machine Learning" techniques were used for*
31 *upscaling observations. I didn't see an explanation of how this was done in the text or supplemental*
32 *material. As there are many, many, many different machine learning approaches, I ask the authors to*
33 *revise the text associated with this to explain what technique was used. What the inputs were, what the*
34 *outputs from this are, and how the algorithm was trained (if relevant). A reference(es) for the technique*
35 *used should also be given. The relevant equations should be given if the approach is new. When making*
36 *these changes, please keep in mind that readers of the manuscript should have sufficient knowledge of*
37 *what you did so that they could reproduce your approach.*

38

39 **We have rewritten the section describing the estimation of spatial parameters and put more**
40 **emphasis on applied the machine learning methodology:**

41

42 Lines 447 – 464: For spatial parameterization of the DMMF model, we predicted land cover, soil
43 properties and burrow distribution onto the hillslope catchments using machine learning techniques.
44 We used the approach Meyer et al. 2018. The most important predictors were selected by forward
45 feature selection. The quality of the random forest models was assessed by Leave-Location-Out cross
46 validation. We trained the model stepwise, using in-situ data collected from seven of the hillslope
47 catchments and validated the model using in-situ data from the remaining hillslope catchment (Meyer et
48 al., 2018). The prediction was done at 0.5 m spatial resolution. We used the WorldView-2 layers obtained
49 with a single license from GAF, NDVI, DEM, DSM, slope and roughness as predictors. The PAN-
50 sharpening of the WV-2 layers was done by GAF.

51 For the area-wide prediction of burrow locations across the hillslope catchments, we used the burrow
52 presence and absence data (section 3.1) as the response data within the RF models. The accuracy was
53 0.82 for PdA, 0.77 for SG, 0.75 for LC and 0.85 for NA. The prediction of soil properties was done using
54 soil properties estimated along the track line (see section 3.1) as response data within the RF models.
55 All of the models reached a high accuracy (see Table A1).

56 To obtain land cover classification, we used as the response within the RF models the land cover
57 measured in-situ. The classes were soil without rocks, rocks, biocrusts, grass/herbs, shrubs and trees.
58 Predictor values for each class were extracted from at least 100 polygons per site and class. The
59 accuracy of the RF models was 0.71 for PdA, 0.81 for SG, 0.83 for LC and 0.75 for NA.

60

61 *Second, please add a statement in the acknowledgments (or main text) about where the data and*
62 *models used in the study can be accessed. For example, is there a link (or DOI preferably) for the source*
63 *code and data used in the study? Please also do this for the machine-learning code used. Data or*
64 *software archiving (with a DOI) can easily be done through <https://zenodo.org> or via GFZ data services*
65 *(for EarthShape related research) - note however, the copyright of the erosion modeling software used*
66 *must be honored and you may not be allowed to repost it (hopefully not).*

67

68 **We included in the acknowledgments where the data used, model output and model code can**
69 **be accessed:**

70

71 **Lines 826 – 829: Code/Data availability:** The estimated soil properties (DOI: 10.5678/wsrb-9f70),
72 modelled sediment redistribution (DOI: 10.5678/32wa-d179) and model code ([https://gitlab.uni-](https://gitlab.uni-marburg.de/fb19/ag-bendix/model-sediment-redistribution-caused-by-bioturbating-animals)
73 [marburg.de/fb19/ag-bendix/model-sediment-redistribution-caused-by-bioturbating-animals](https://gitlab.uni-marburg.de/fb19/ag-bendix/model-sediment-redistribution-caused-by-bioturbating-animals)) was
74 published via LCRS data services.

75

76

77

78

79

80

81

82

83 **Mammalian bioturbation amplifies rates of both hillslope sediment erosion and accumulation**
84 **along Chilean climate gradient**

85 *Paulina Grigusova*¹, *Annegret Larsen*², *Roland Brandl*³, *Camilo del Río*^{4,5}, *Nina Farwig*⁶, *Diana Kraus*⁶,
86 *Leandro Paulino*⁷, *Patricio Plischoff*^{4,8,9}, *Jörg Bendix*¹

87
88

89 ¹ Laboratory for Climatology and Remote Sensing, Department of Geography, University of Marburg,
90 35037 Marburg, Germany; paulina.grigusova@staff.uni-marburg.de (P.G.); bendix@geo.uni-
91 marburg.de (J.B.)

92 ² Soil Geography and Landscape, Department of Environmental Sciences,
93 Wageningen University & Research, 6700 AA Wageningen, The Netherlands; annegret.larsen@wur.nl

94 ³ Animal Ecology, Department of Biology, University of Marburg, 35032 Marburg, Germany;
95 brandlr@biologie.uni-marburg.de

96 ⁴ Facultad de Historia, Geografía y Ciencia Política, Instituto de Geografía, Pontificia Universidad Católica
97 de Chile, 782-0436 Santiago, Chile; cdelriol@uc.cl

98 ⁵ Centro UC Desierto de Atacama, Pontificia Universidad Católica de Chile, 782-0436 Santiago, Chile

99 ⁶ Conservation Ecology, Department of Biology, University of Marburg, 35047 Marburg, Germany;
100 diana.kraus@biologie.uni-marburg.de (D.K.); nina.farwig@biologie.uni-marburg.de (N.F.)

101 ⁷ Facultad de Agronomía, Universidad de Concepción, 3780000 Chillán, Chile; lpaulino@udec.cl

102 ⁸ Facultad de Ciencias Biológicas, Departamento de Ecología, Pontificia Universidad Católica de Chile,
103 8331150 Santiago, Chile; plischoff@uc.cl

104 ⁹ Center of Applied Ecology and Sustainability (CAPES), Pontificia Universidad Católica de Chile,
105 8331150 Santiago, Chile; plischoff@uc.cl

106

107 Corresponding author:

108 Paulina Grigusova

109 paulina.grigusova@staff.uni-marburg.de

110

111

112

113

114

115

116

117

118

119

120

121

122

123

124 **Abstract**

125 Animal burrowing activity affects soil texture, bulk density, soil water content and redistribution of
126 nutrients. All of these parameters in turn influence sediment redistribution, which shapes the earth
127 surface. Hence it is important to include bioturbation into hillslope sediment transport models. However,
128 the inclusion of burrowing animals into hillslope-wide models has thus far been limited, and largely
129 omitted vertebrate bioturbators, which can be major agents of bioturbation, especially in drier areas.
130 Here, we included vertebrate bioturbator burrows into a semi-empirical Morgan-Morgan-Finney soil
131 erosion model to allow a general approach to for assessing the impacts of bioturbation on sediment
132 redistribution within four sites along the Chilean climate gradient. For this, we predicted the distribution
133 of burrows by applying machine learning techniques in combination with remotely sensed data into the
134 hillslope catchment. Then, we adjusted the spatial model parameters at predicted burrow locations
135 based on field and laboratory measurements. We validated the model using field sediment fences. We
136 estimated the impact of bioturbator burrows on surface processes. Lastly, we analyse how the impact
137 of bioturbation on sediment redistribution depends on the burrow structure, climate, topography, and
138 adjacent vegetation.

139 Including bioturbation greatly increased model performance and demonstrates the overall importance
140 of vertebrate bioturbators in enhancing both sediment erosion and accumulation along hillslopes, though
141 this impact is clearly staggered according to climatic conditions. Bioturbation had contrasting effects on
142 sediment redistribution in arid than in semi-arid and Mediterranean, as well as in humid climate zone.

143 Burrowing vertebrates increased sediment accumulation by 137.8 % \pm 16.4 % in the arid zone (3.53 kg
144 $\text{ha}^{-1} \text{ year}^{-1}$ vs. 48.79 kg $\text{ha}^{-1} \text{ year}^{-1}$), sediment erosion by 6.5 % \pm 0.7 % in the semi-arid zone (129.16 kg
145 $\text{ha}^{-1} \text{ year}^{-1}$ vs. 122.05 kg $\text{ha}^{-1} \text{ year}^{-1}$) and sediment erosion by 15.6 % \pm 0.3 % in the Mediterranean zone
146 (4602.69 kg $\text{ha}^{-1} \text{ year}^{-1}$ vs. 3980.96 kg $\text{ha}^{-1} \text{ year}^{-1}$). Bioturbating animals seem to play only a negligible
147 role in the humid zone. Within all climate zones, bioturbation did not uniformly increase erosion or
148 accumulation within the whole hillslope catchment. This depended on adjusting environmental
149 parameters. Bioturbation increased erosion with increasing slope, sink connectivity and topography
150 ruggedness, decreasing vegetation cover and soil wetness. Bioturbation increased sediment
151 accumulation with increasing surface roughness, soil wetness and vegetation cover.

152
153
154
155
156
157
158
159
160
161
162
163
164

165 1. Introduction

166 Bioturbation was shown to shape the land surface (Hazelhoff et al., 1981; Istanbuluoglu, 2005; Taylor
167 et al., 2019; Tucker and Hancock, 2010; Whitesides and Butler, 2016; Wilkinson et al., 2009; Corenblit
168 et al., 2021) by influencing surface microtopography (Reichman and Seabloom, 2002; Kinlaw and
169 Grasmueck, 2012; Debruyne and Conacher, 1994), and soil properties such as soil porosity, permeability
170 and infiltration (Reichman and Seabloom, 2002; Yair, 1995; Hancock and Lowry, 2021; Ridd, 1996; Hall
171 et al., 1999; Coombes, 2016; Larsen et al., 2021). Cumulatively, these modifications lead to changes in
172 sediment redistribution (Gabet et al., 2003; Nkem et al., 2000; Wilkinson et al., 2009) and hence have
173 the potential to affect surface topography and nutrient redistribution on large spatial and temporal scales.
174 To quantify these effects, the shared role of climate, landscape characteristics and burrowing dynamics
175 on sediment redistribution needs to be understood.

176 On a local scale, currently used field methods to monitor sediment redistribution under real-life condition
177 are mainly erosion pins, splash boards, or rainfall simulators (Imeson and Kwaad, 1976; Wei et al., 2007;
178 Le Hir et al., 2007; Li et al., 2019a; Li et al., 2019b; Li et al., 2018; Voiculescu et al., 2019; Chen et al.,
179 2021; Übernickel et al., 2021a). The monitoring of box experiments yields a high spatio-temporal
180 resolution, and can also be linked with mathematical equations, such as random walks (Boudreau, 1986;
181 Wheatcroft et al., 1990), stochastic differential equations (Boudreau, 1989; Milstead et al., 2007), finite
182 difference mass balancing (Soetaert et al., 1996; François et al., 1997) or Markov chain theory (Jumars
183 et al., 1981; Foster, 1985; Trauth, 1998; Shull, 2001) to describe sediment redistribution.

184 Previously used methods have, however, several limitations when studying bioturbation. Field
185 measurements likely lead to an underestimation of sediment fluxes, as they are one-time or seasonal
186 measurements, and thus do not capture the continuous excavation of the sediment by the animal
187 (Grigusova et al., 2022) at a high temporal resolution. Box experiments and from them derived
188 mathematical equations describe bioturbation as an isolated process and ignore adjacent environmental
189 parameters (such as climate or vegetation). However, the field measurements showed both, positive
190 (Hazelhoff et al., 1981; Black and Montgomery, 1991; Chen et al., 2021) and negative impact of
191 bioturbation on erosion (Imeson and Kwaad, 1976; Hakonson, 1999). Also, previous field based studies
192 observed an increased bioturbation activity with higher (Milstead et al., 2007; Meserve, 1981; Tews et
193 al., 2004; Wu et al., 2021; Ferro and Barquez, 2009), but also with lower vegetation cover (Simonetti,
194 1989; Zhang et al., 2020; Zhang et al., 2019; Qin et al., 2021). Furthermore, soil mixing rates are not
195 homogenous throughout the year but depend on the animal phenological cycles (Eccard and Herde,
196 2013; Jimenez et al., 1992; Katzman et al., 2018; Malizia, 1998; Morgan and Duzant, 2008; Monteverde
197 and Piudo, 2011; Gray et al., 2020; Yu et al., 2017).

198 Another approach offer raster-based soil erosion and landscape evolution models which integrate co-
199 dependencies between bioturbation relevant environmental parameters (Black and Montgomery, 1991;
200 Meysman et al., 2003; Yoo et al., 2005; Schiffers et al., 2011). Most common soil erosion models are
201 empirical (Wischmeier and Smith, 1978; Williams, 1975; Renard et al., 1991), process-based (Morgan
202 et al., 1998; ROO et al., 1996; Nearing et al., 1989; Beasley et al., 1980), or semi-empirical models, the
203 latter of which are a combination of both (Morgan et al., 1984; Beven and Kirkby, 1979).

204 **Process-based models are based on a mechanistic understanding of the underlying physical, chemical,
205 and biological processes that govern the behaviour of the system being studied. They must be**

206 parametrised for each site; however, these models explicitly represent the governing equations and
207 simulate the system's behaviour by numerically solving these equations. Process-based models are
208 generally considered to be more realistic and accurate than empirical models because they capture the
209 fundamental processes that drive the system's behaviour. However, process-based models can be
210 computationally expensive, require more data and knowledge of system properties, and may require
211 complex numerical algorithms (Morgan et al., 1998; ROO et al., 1996; Nearing et al., 1989; Beasley et
212 al., 1980).

213 Within empirical models, on the other hand, the physical equations are completely replaced by
214 empirically determined equations which only hold for the specific area they are derived for. These
215 models are generally simpler, less computationally expensive, and require more data and knowledge of
216 system properties than process-based models. However, empirical models also tend to be less accurate
217 than process-based models, particularly when applying beyond the range of data used to fit the model.
218 In contrast to physical-based models, empirical models may not be applicable to new or different
219 conditions, as they are based on observed relationships and do not capture the underlying processes
220 that govern system behaviour (Wischmeier and Smith, 1978; Williams, 1975; Renard et al., 1991).

221 **Semi-empirical** models combine the advantages of the both model types (Morgan et al., 1984; Morgan,
222 2001; Morgan and Duzant, 2008; Devia et al., 2015; Lihare et al., 2015).

223 Most landscape models do not yet **implement impacts** of bioturbators on water and sediment fluxes
224 (Brosens et al., 2020; Anderson et al., 2019; Braun et al., 2016; Cohen et al., 2015; Cohen et al., 2010;
225 Carretier et al., 2014; Welivitiya et al., 2019). There are numerous models describing benthic soil mixing
226 (Francois et al. 1997, Francois et al. 2002, Kadko and Heath 1984, Croix et al. 2002), biodiffusion caused
227 by all invertebrate bioturbators (Maysman et al. 2005, Rakotomalala et al. 2015, Morris et al. 2006) or
228 vertical soil mixing and lateral sediment redistribution caused by single invertebrate species (Orvain et
229 al. 2006, Román – Sánchez et al. 2019, Orvain 2005, Orvain 2003, Sanford 2008). However, there are
230 also models which described the impact of bioturbation on sediment redistribution by the vertebrate
231 animal species: such as the impact of pocket gophers on non-linear hillslope diffusion (Gabet 2000) or
232 on the creation of Mima mounds (Gabet et al. 2014). Several models include soil vertical mixing caused
233 by bioturbation and its effect on landscape evolution on a millennial scale. This rather large spatio-
234 temporal scale however means an omission of the natural variability in burrow sizes and densities,
235 climate zones and seasonality. In these models, soil erosion is proportionally increasing with increasing
236 bioturbation, vertical soil mixing rates are uniform, and bioturbation is positively linked with vegetation
237 cover (Temme and Vanwalleghem, 2016; Vanwalleghem et al., 2013; Yoo and Mudd, 2008; Pelletier et
238 al., 2013). None of the previous studies included vertebrate bioturbator burrows of various sizes and
239 spatial distribution by adjusting the soil properties and topography into a raster-based area-wide soil
240 erosion model. This approach would enable to understand impact of all vertebrate bioturbators by
241 considering the spatial distribution and variable impacts of bioturbator burrows on sediment
242 redistribution. For this, bioturbation has to be included into erosion models at a spatial resolution which
243 allows to imitate the surface processes occurring within and near the burrow, and at a temporal
244 resolution which captures the animal daily burrowing behaviour.

245 A suitable model which can be extended to include continuous bioturbating activity is the semi-empirical
246 Morgan – Morgan – Finney soil erosion model (Morgan et al., 1984; Morgan, 2001). This model was

247 successfully tested in several climate zones and land use types, such as Mediterranean sites (Jong et
248 al., 1999), rainfed agrosystems, fields and pastures (López-Vicente et al., 2008), East-African Highlands
249 (Vigiak et al., 2005) or humid forests (Vieira et al., 2014). One of the recently developed improvements
250 of this model is the Daily Morgan – Morgan – Finney model (DMMF), which introduces subsurface flow,
251 vegetation structures (type, size, height, root depth), and enables modelling at a high spatial (0.5 m) and
252 temporal (daily) resolution (Choi et al., 2017). These improvements yield the potential to integrate the
253 bioturbation into the model, as the burrowing activity is not constant and depends on vegetation structure
254 (Tews et al., 2004; Ferro and Barquez, 2009).

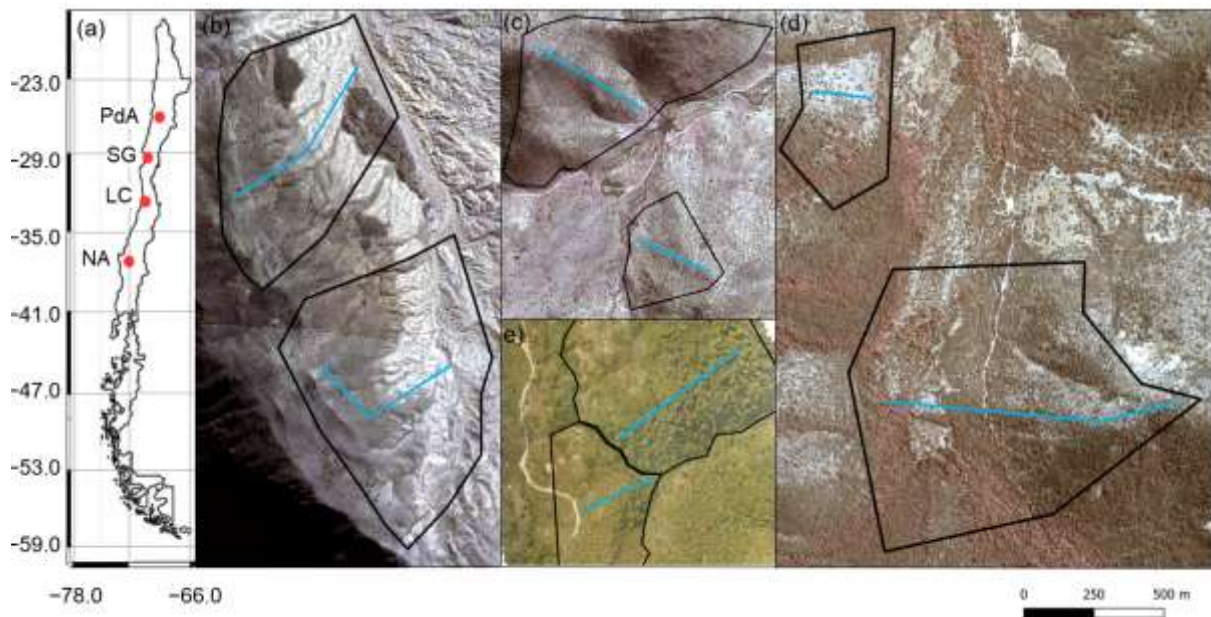
255 In this study, we include vertebrate bioturbator burrows into a semi-empirical soil erosion model (DMMF)
256 at a daily temporal and 0.5 m spatial resolution. For this, we predict the distribution of burrows by
257 applying machine learning techniques in combination with using remotely sensed data as predictors.
258 Then, we adjust soil properties, topography and vegetation properties at predicted burrow locations
259 based on field and laboratory measurements. We validate the model using field sediment fences. We
260 run the model for a time period of 6 years, once with and without burrow adjustments. We estimate the
261 impact of bioturbator burrows on sediment redistribution (including accumulation, erosion, and
262 excavation), and surface runoff within four sites along the Chilean climate gradient. Lastly, we analyse
263 how the impact of bioturbation on sediment redistribution depends on the burrow structure, climate,
264 topography, and adjacent vegetation. Our study shows the importance of including bioturbation into
265 erosion modelling, and describes the interplay between bioturbation, environmental parameters such
266 as... and sediment redistribution.

267

268 2. Study area

269 Our study was performed along a climate and vegetation gradient in Chile (Übernicket et al., 2021b),
270 comprising four study sites in the Chilean Coastal Cordillera: Pan de Azúcar (PdA) National Park (NP),
271 Santa Gracia (SG), La Campana (LC) NP, and Nahuelbuta (NA) NP (Fig. 1). PdA NP is located in the
272 arid zone in a fog-laden environment in the southern part of the Atacama Desert, with almost no rainfall.
273 The vegetation cover is less than 5 % and dominated by small desert shrubs, several types of cacti and
274 biocrusts (Lehnert et al., 2018). SG is a natural reserve located in the semi-arid zone near La Serena,
275 which is dominated by goat grazing. The vegetation consists of shrubs and cacti, covering up to 40 %
276 of the study area. LC NP is part of the Mediterranean-type climate zone in the Valparaiso Region and is
277 also affected by cattle. The study site is dominated by an evergreen sclerophyllous forest with endemic
278 palms. The canopy reaches a height of up to 9 m, and the understory consists of deciduous shrubs and
279 herbs. NA is located in the humid-temperate zone and characterized by a dense evergreen *Araucaria*
280 forest comprising broadleaved trees with heights of up to 14 m. The ground is covered by bamboo,
281 shrubs, and herbs (Bernhard et al., 2018; Oeser et al., 2018). The most common bioturbating vertebrate
282 animal species recorded within these sites are carnivores of the family Canidae (*Lycalopex culpaeus*,
283 *Lycalopex griseus*) as well as rodents of the families Abrocomidae (*Abrocoma bennetti*), Chnichillidae
284 (*Lagidium viscacia*), Cricetidae (*Abrothrix andinus*, *Phyllotis xanthopygus*, *Phyllotis limatus*, *Phyllotis*
285 *darwini*) and Octogontidae (Cerqueira, 1985; Jimenez et al., 1992; Übernicket et al., 2021a).

286

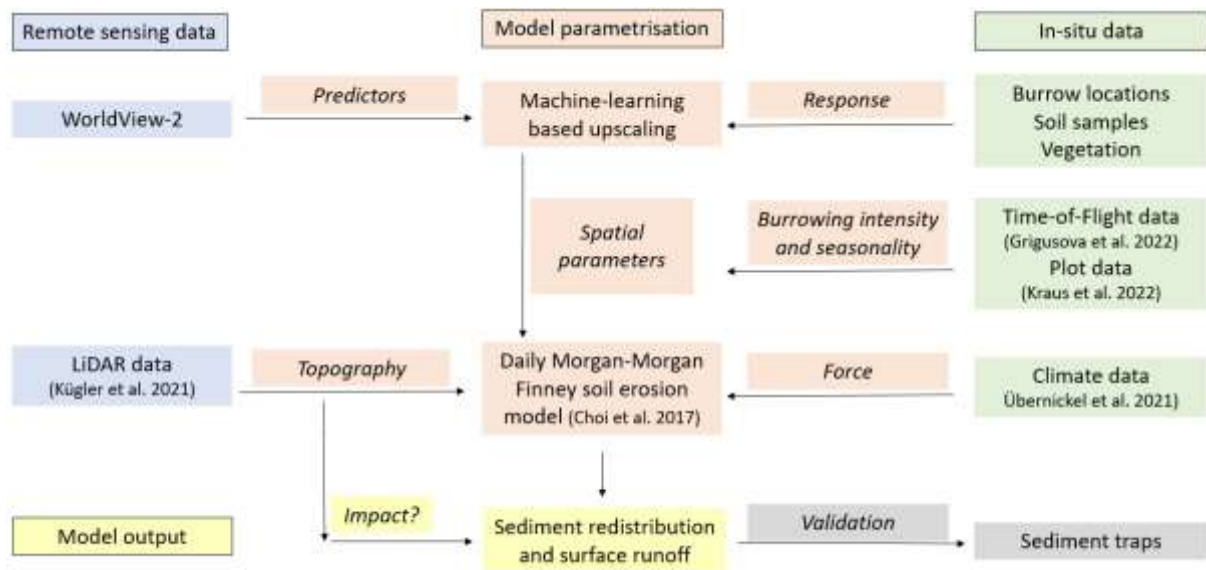


287
 288 **Figure 1.** Study area and study sites. Black lines outline the hillslope catchments. Along the blue lines,
 289 the in situ data (mound locations, soil samples, vegetation mapping) were collected. (a) Position of the
 290 study sites along the climate gradient. PdA = Pan de Azúcar, SG = Santa Gracia, LC = La Campana,
 291 NA = Nahuelbuta; Positions of plots in (b) PdA; (c) SG; (d) LC; and (e) NA. The background image is an
 292 RGB-composite calculated from WorldView-2 satellite imagery. Images were obtained with single
 293 license from GAF AG. Scale bar is the same for (b), (c), (d) and (e).

294
 295 **3. Methodology**

296 We combined semi-empirical soil erosion modelling with in-situ measurements, remote sensing data
 297 and machine learning methods (Fig. 2). Along 8 hillslope catchments within 4 climate zones we mapped
 298 locations of burrows, estimated the vegetation cover and extracted soil samples. We analyzed the soil
 299 samples in the laboratory. Then we used remote sensing datasets and machine learning to upscale
 300 burrow distribution, vegetation cover and soil properties into the hillslope catchments. The hillslope
 301 catchment-wide predictions, the topographical information retrieved from LiDAR data (Kügler et al.,
 302 2022) and the climate information retrieved from climate stations were the input parameters for our soil
 303 erosion model. We ran the model with and without bioturbation. We included the bioturbation into the
 304 model by adjusting the input parameters at the predicted burrow locations, by including the continuous
 305 burrowing activity and soil mixing (Grigusova et al., 2021), and the seasonality (Kraus et al., 2022).and
 306 the animal phenological cycle as found in (Jimenez et al., 1992). The models were validated using self-
 307 constructed sediment traps. We studied the modeled surface runoff and sediment redistribution. Lastly,
 308 we analyzed if and how the impact of bioturbation on sediment redistribution depends on environmental
 309 parameters (topography, landscape connectivity and vegetation).

310
 311



312

313 **Figure 2.** Flow chart of our study. Green color indicates in-situ input data, blue indicates remote sensing
 314 input data. Red indicates Model parametrization. Yellow indicates model output and analysis. Grey
 315 indicates model validation.

316

317 3.1 In-situ data

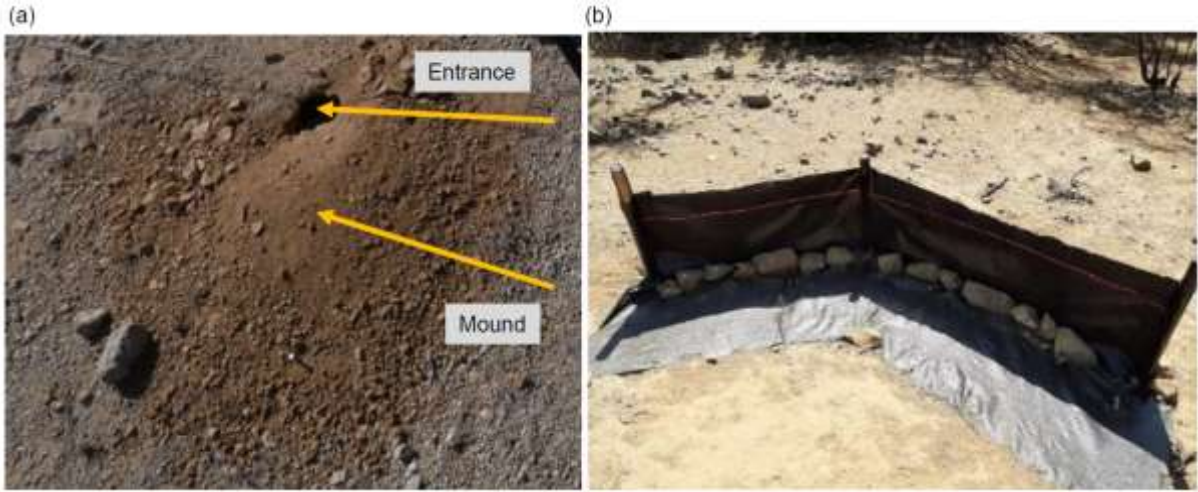
318 The study set-up consisted of eight hillslope catchments: one north-facing and one south-facing hillslope
 319 catchment per study site. We defined a line with a width of one meter from the top to the base of each
 320 hillslope catchment (see blue line, Fig. 1). We subdivided the track into tiles of 1 m². We saved the GPS
 321 information of each tile.

322 Within each tile of the line, we mapped burrow presence, land cover and extracted soil samples. A
 323 burrow consisted of an entrance and a mound (Fig. 3a). Each 1 m² tile with a burrow was described as
 324 a presence data point, tiles without a burrow as absence data points. We noted the size of the burrow,
 325 vegetation cover and land cover types (bare soil, herbs, shrubs, trees) within the tile. We extracted 162
 326 soil samples from soil without a mound at a depth of 10 cm. Additionally, we took a photo of the surface
 327 every second tile along the track.

328 To validate the model output, we set up sediment traps (Fig. 3b), with six traps per site, two of which
 329 were located at the hillslope catchment base and four were located on two random positions within the
 330 hillslope catchment. The sediment traps consisted of geotextile vertically attached to wooden poles for
 331 stability. The traps had a length of 2 m – 5 m, a width of ~1.5 m and a height of ~1 m. 1.5 m of geotextile
 332 was laid down at the surface uphill the wooden poles to enable the collection of sediment. The sediment
 333 accumulated within the traps was collected after 1 year and its mass [cm³] and dry weight [kg] were
 334 estimated.

335 Climate information was retrieved from climate stations located adjacent to the hillslope catchments
 336 which provide climate data in 5 minute intervals (Übernicket et al. 2021). To force the model on an hourly
 337 basis, hourly air temperature, precipitation total and intensity, wind speed, wind direction and humidity
 338 was calculated for the study period from 1st April 2016 to 1st December 2021. Evapotranspiration was
 339 estimated by the Penman-Monteith equation (Penman, 1948).

340



341
 342 **Figure 3.** In-situ constructions. (a) Example of a burrow consisting of burrow entrance and mound. (b)
 343 Fence construction used for the collection of eroded sediment to validate the model. Both photos by
 344 Paulina Grigusova.

345

346 3.2 Estimation of soil properties

347 We estimated several soil properties from the soil samples and photos collected in-situ (Grigusova et
 348 al., 2022). We estimated the rock coverage on the surface and debris from the photos taken every
 349 second tile. For this, the photos were firstly classified into 5 classes. The classification was unsupervised
 350 using k-means (Fig. A1). Then we calculated the ratio of pixels classified as skeleton and / or debris to
 351 the overall amount of all pixels to determine the amount of both parameters in percent.

352 In the lab, we estimated soil water content, bulk density, soil particle density, soil texture (sand, silt, clay,
 353 coarse / middle / fine sand, coarse / middle / fine silt), soil skeleton, organic matter and organic carbon.
 354 Gravimetric soil water content [%] (GSWC) described the mass of water within the soil sample and was
 355 estimated as in Eq (1):

$$356 \text{GSWC} = \frac{(S_m - S_d)}{S_d} * 100 \quad , \quad (1)$$

357 where S_m [g] is the mass of moist soil measured directly after the extraction and S_d [g] is the mass of
 358 soil dried at 105 °C for at least 24 hours. Bulk density [g cm^{-3}] (BD) was calculated as following:

$$359 \text{BD} = \frac{S_d}{S_v} \quad , \quad (2)$$

360 where S_v [cm^{-3}] is the volume of the sample. Soil particle density [g cm^{-3}] (SPD) was calculated as in Eq
 361 (3):

$$362 \text{SPD} = \frac{dm}{S_v} \quad , \quad (3)$$

363 where dm [g] is the dry mass of soil particles excluding pores.

364 Particle size distribution [%] – clay (< 0.002 mm), coarse, middle and fine silt (0.002 mm to 0.02 mm),
 365 and coarse, middle and fine sand (0.02 mm to 2 mm) was estimated using a PARIO method (Durner et
 366 al., 2017). Soil skeleton was estimated as the ratio of particles with a diameter above 2 mm. Ratio of
 367 organic matter (OM) was estimated as in Eq. (4)

$$368 \text{OM} = 1 - \frac{S_c}{S_d} \quad , \quad (4)$$

369 where S_c is the weight [g] of the sample dried at 500 °C for 16 hours.

370 We used pedotransfer functions to determine porosity, saturated soil moisture, hydraulic conductivity,
 371 water content at field capacity, and permanent wilting point. Pore ratio (θ_s) was estimated from bulk and
 372 particle density as in Eq. (5):

$$373 \theta_s = \frac{BD}{SPD} \quad (5)$$

374 Saturated water content [g g^{-1}] (W_s) was estimated as in Eq. (6):

$$375 W_s = \theta_s \frac{\rho_w}{BD} \quad (6)$$

376 where ρ_w [g cm^{-3}] is the density of water which is set to be 1 g cm^{-3} (Pollacco, 2008).

377 Hydraulic conductivity K_s [m s^{-1}] was estimated as in Eq. (8):

$$378 K_s = 1.15741 * 0.0000001 * \exp(x) \quad (7)$$

379 where x for sandy soil is:

$$380 x = 9.5 - 1.471 * (BD * BD) - 0.688 * OM + 0.0369 * (OM * OM) - 0.332 * CS \quad (8)$$

381 and x for loamy and clayey soils is:

$$382 x = -43.1 + 64.8 * BD - 22.21 * (BD * BD) + 7.02 * OM - 0.1562 * (OM * OM) + 0.985 * \ln(OM) -$$

$$383 0.01332 * C * OM - 4.71 * BD * CS \quad (9)$$

384 where C is percentage of clay and CS is percentage of clay and silt (Wösten, 1997). To estimate water
 385 content at field capacity [%] (FC) and permanent wilting point (PWP), we applied functions by (Tomasella
 386 et al., 2000) as these were developed for South American soils:

$$387 FC = 4.046 + 0.426 * Si + 0.404 * C \quad (10)$$

$$388 PWP = 0.91 + 0.15 * Si + 0.396 * C \quad (11)$$

389 where Si is the percentage of silt.

390

391 3.3 Processing of remote sensing data

392 The digital elevation models (DEM) were calculated from the LiDAR data (Kügler et al., 2022; Horn,
 393 1981) at a resolution of 0.5 m. Slope was calculated according to Horn (1981). Manning's surface
 394 roughness coefficient was estimated following (Li and Zhang, 2001). Topographic position index (TPI)
 395 and Topographic ruggedness index (TRI) were calculated according to (Wilson et al., 2007). **TPI subtract**
 396 **the mean elevation of pixels in a specified range from the elevation of the central pixel. Positive values**
 397 **represent hills while negative values represent valleys. The TRI adds together the elevation differences**
 398 **between a grid cell and its eight neighbours. It measures the relative level of topography irregularity, the**
 399 **higher the value, the more irregular the topography.** Plan and profile curvature were determined after
 400 (Zevenbergen and Thorne, 1987). Connectivity indices, Sinks, Wetness index, Flow direction, Flow path,
 401 Catchment slope and Catchment were calculated in SAGA GIS.

402 Single license stereo WorldView-2 images with a resolution of 0.5 m were retrieved from GAF Munich
 403 GmbH. The topographic correction of WorldView-2 images was done using the LiDAR data, solar
 404 elevation angle, solar zenith angle and azimuth angle according to Goslee (2019). The digital surface
 405 models (DSMs) were calculated from the stereo images. Additionally, we extracted single bands and
 406 calculated the normalized difference vegetation index (NDVI).

407

408 3.4 The erosion model

409 3.4.1 Daily Morgan-Morgan-Finney model

410 The DMMF model is a combined soil erosion model used to estimate surface runoff and sediment flux
411 on a field scale on a daily basis. Spatially, the DMMF model represents an area as several
412 interconnected elements (e.g. pixels) of uniform topography, soil characteristics, land cover type, and
413 vegetation structure. Through coupling, the model operates with flow direction algorithms: each element
414 receives water and sediments from upslope elements and delivers the generated surface runoff and
415 eroded soils to downslope elements. On a temporal scale, the model estimates surface runoff and
416 sediment flux of each element on a daily basis. The model input parameters include climate, topography,
417 soil properties and land cover information (Choi et al., 2017). Data pre-processing, modelling and
418 analysis (see Fig. 2) was done in R statistic environment. The raster data were cropped to the size of
419 the hillslope catchments (Fig. 1). Input parameters are listed in Table 1 and plotted in Fig. A2.

420 During the model simulation, water and sediment are transferred from pixels located at higher elevations
421 to pixels situated at lower elevations. This occurs in two stages: The first stage is the hydrological phase
422 where the model calculates surface runoff which happens when the amount of surface water input
423 exceeds the water-holding capacity. The amount of surface runoff is computed by taking the infiltration
424 capacity of the surface, the volume of surface water input, and the fraction of the impervious area of a
425 pixel into account. Infiltration capacity represents the maximum amount of surface water that can
426 penetrate the subsurface layer. It is determined by the percentage of the impervious area and the
427 available pore space.

428 The second stage is the sediment phase, where the model estimates the sediment budget for each
429 particle size class, based on the surface conditions. The model calculates the detachment and
430 deposition of sediments in a step-by-step process. The sources of sediments are detached particles
431 from the pixel itself due to rainfall and surface runoff, and delivered soil particles from higher elevation
432 pixels. The detachment of soil particles by rainfall occurs when raindrops hit the ground with enough
433 energy to detach soil particles from the surface. Rainfall has different impacts on areas with and without
434 canopy cover, as canopy cover changes the kinetic energy of raindrops.

435 The amount of soil particles detached by raindrops is calculated based on the soil particle detachability,
436 the percentage of each particle size class, the bare soil surface area, and the kinetic energy of effective
437 rainfall. The amount of detached soil particles by surface runoff is calculated based on the soil particle
438 detachability, the amount of runoff, the slope angle of the pixel, and the proportion of the bare surface
439 area. The third source of sediment is from higher elevation pixels and is averaged by the surface area
440 of the pixel.

441 Once sediments are delivered to the surface runoff, a portion of the suspended sediments settles to the
442 bottom due to gravitational force. To calculate this settling, the model requires the flow velocity of the
443 runoff and the settling velocity of each particle size class, which are influenced by the flow depth, slope
444 angle of the pixel, and Manning's roughness coefficient (Choi et al. 2019).

445

446 **3.4.2 Estimation of spatial parameters**

447 For spatial parameterization of the DMMF model, we predicted land cover, soil properties and burrow
448 distribution onto the hillslope catchments using machine learning techniques.

449 We used the approach Meyer et al. 2018. The most important predictors were selected by forward
450 feature selection. The quality of the random forest models was assessed by Leave-Location-Out cross

451 validation. We trained the model stepwise, using in-situ data collected from seven of the hillslope
452 catchments and validated the model using in-situ data from the remaining hillslope catchment (Meyer et
453 al., 2018). The prediction was done at 0.5 m spatial resolution. We used the WorldView-2 layers obtained
454 with a single license from GAF, NDVI, DEM, DSM, slope and roughness as predictors. The PAN-
455 sharpening of the WV-2 layers was done by GAF.

456 For the area-wide prediction of burrow locations across the hillslope catchments, we used the burrow
457 presence and absence data (section 3.1) as the response data within the RF models. The accuracy was
458 0.82 for PdA, 0.77 for SG, 0.75 for LC and 0.85 for NA. The prediction of soil properties was done using
459 soil properties estimated along the track line (see section 3.1) as response data within the RF models.
460 All of the models reached a high accuracy (see Table A1).

461 To obtain land cover classification, we used as the response within the RF models the land cover
462 measured in-situ. The classes were soil without rocks, rocks, biocrusts, grass/herbs, shrubs and trees.
463 Predictor values for each class were extracted from at least 100 polygons per site and class. The
464 accuracy of the RF models was 0.71 for PdA, 0.81 for SG, 0.83 for LC and 0.75 for NA.

465 The vegetation height measured in plots was averaged for each class per site. All pixels classified as
466 respective class were assigned the same vegetation height information. Vegetation density was
467 estimated per hillslope catchment as the amount of vegetation individuals per m². Vegetation diversity
468 was calculated by Shannon index (Shannon, 1948). The interception area was the area not covered by
469 vegetation (herbs, shrubs or trees).

470

471

472 3.4.3 Inclusion of bioturbation

473 In the grid cells with predicted burrow locations, we adapted the values of input parameters to include
474 bioturbation. The adaptations varied with climate zone and burrow size. The size, geometric structure
475 and excavation rates of burrowing animals were previously estimated at a high spatial and temporal
476 resolution (Grigusova et al., 2022). Based on this results, we firstly adjusted the microtopography. We
477 modified the layer depth to represent burrow entrance and elevation to represent animal mound. Mounds
478 were always located downslope of burrow entrances in the direction of flow.

479 Secondly, we adjusted the soil properties. Soil properties texture and organic carbon were estimated
480 from soil extracted from mounds in Kraus et al. (2022). In this study we additionally estimated bulk
481 density, initial water content, soil skeleton, porosity, saturated water content, available water capacity
482 and water content at field capacity from the same dataset (see section 3.2). We calculated the median
483 value of each property for the samples extracted from mounds and for the samples extracted from soil
484 without mounds. Then, we estimated the change in percent between these two values. This was then
485 used to adjust the soil property for each pixel including a mound.

486 Thirdly, modelled mound pixels had to be cleared from ground vegetation cover. For this, we removed
487 ground vegetation cover from pixels with burrow locations and decreased ground vegetation cover,
488 height, diameter and amount of ground vegetation individuals from adjacent pixels as measured in situ.
489 Then, the amount of rocks and debris was set as estimated from soil samples (section 3.2)

490 Animal activity has been found to be highly variable throughout the year (Grigusova et al., 2022; Kraus
491 et al., 2022). The density of burrows does not stay stable throughout the year but increases or decreases

492 depending on the season and climate zone. We therefore artificially removed or added burrows into the
 493 hillslope catchments at the particular seasons. For this, we adapted the density of soil, the topography
 494 and vegetation cover accordingly. We created a 3D-model of the burrow structure, adjusted subsurface
 495 soil properties and properties of soil excavated to the surface; the removed vegetation within the pixel
 496 with a predicted burrow and decreased adjacent vegetation cover. Animal burrowing activity varies
 497 throughout the course of the year, and there is a three-month period during which they are mostly active,
 498 which we considered using/doing xxx

499 Lastly, we also included the vertical movement of sediment particles from deeper soil layers to the
 500 surface in dependence on climate. Animals were found to reconstruct their burrows after each rainfall
 501 event (Grigusova et al., 2022). Corresponding with these findings, we increased the entrance depth and
 502 mound height by 30% after each rainfall event, which represents the averaged value found in the
 503 previous study (Grigusova et al., 2022).

504 For the validation, we ran the model for the time periods between the installation of sediment fences
 505 and the collections of sediment. We compared the mass and weight of modelled and collected sediment
 506 and estimated R² and RMSE. To test the importance of the inclusion of individual bioturbation
 507 parameters into the model, we ran the model under 4 conditions: (i) No burrows; (ii) Solely entrances;
 508 (iii) Solely mounds; (iv) Entire burrows (entrances and mounds).

509

510 **Table 1.** Model input layers and respective changes to layer values at the predicted burrow locations.
 511 Ground vegetation was removed from the respective pixels, while tree canopy was not changed. The
 512 values were estimated as described in 3.5.2. Using the adjusted values, we calculated
 513 evapotranspiration using the Penman-Monteith equation, surface roughness from the elevation layer,
 514 and hydraulic conductivity, water content at field capacity and saturated water content using
 515 pedotransfer functions.

Derivation	Parameter	Units	Pixel value at burrow locations			
			PdA	SG	LC	NA
DEM	Elevation	m asl	+0.24	+0.23	+0.36	+0.19
	Surface roughness	-	-	-	-	-
	Depth	m	-0.23	-0.41	-0.22	-0.04
Soil samples	Water content	%	+120	-6	-68	-62
	Bulk density	g cm ⁻³	-	-6	-17	-
	Sand	%	-29	-12	+57	-43
	Silt	%	+54	+22	+23	ns
	Clay	%	+145	+44	+19	-73
	Organic carbon	%	+168	+72	+105	+25
Pedotransfer functions	Hydraulic conductivity	m s ⁻¹	-	-	-	-
	Water content at field capacity	%	-	-	-	-
	Saturated water content	%	-	-	-	-
	Ground vegetation cover	%	0	0	0	0

Land cover classification	Soil and debris	%	100	100	100	100
	Skeleton	%	0	0	0	0
	Average plant height	m	0	0	0	0
	Average plant diameter	m	0	0	0	0
	Number of plants	n m ⁻²	0	0	0	0

516

517 3.5 DMMF model sensitivity test

518 We conducted a sensitivity test to identify those input parameters which significantly influence the model
519 output. For this, we first estimated the mean value of each input parameter. Then, we created an artificial
520 hillslope catchment of 100 m * 100 m. To start the test, each pixel received the mean value of each
521 parameter. We ran the model for one rainfall event. Then, we stepwise changed the single input
522 parameter values from their minimum to their maximum values while we did not adjust any other
523 parameters. To quantify the significance of the input variations, we conducted a t-test (Table A2). For
524 this, we compared the amount of redistributed sediment of each model run to the first model run.

525

526 3.6 Impact of burrows on surface processes

527 We estimated burrow density, as a ratio of pixels with predicted burrows to all pixels. Additionally, we
528 calculated the ratio of pixels which are part of a burrow aggregation to all pixels which include a burrow.
529 Burrow aggregation describes at least 4 neighboring pixels with predicted burrows. We calculated the
530 amount of excavated sediment as a sum of burrow density and the burrow excavation rate as estimated
531 in Grigusova et al. (2022).

532 To estimate the impact of burrows on sediment redistribution and surface runoff, we ran the DMMF
533 model for the time period from 1st April 2016 until 31th December 2021 for all hillslope catchments. We
534 ran the model (i) with no burrows and (ii) with entire burrows. We estimated (i) sediment redistribution
535 (accumulation - erosion) and (ii) surface runoff. We analyzed the redistribution and runoff on the plot (1
536 m²) and hillslope catchment (1 ha) scale.

537 Lastly, to analyze under which biotic and abiotic environmental parameters (topography, vegetation
538 cover) the bioturbation enhances sediment erosion or accumulation, we set-up a generalized additive
539 model (GAM) (Wood, 2006). For this, we first subtracted the output of the model with no burrows from
540 the output of the model with entire burrows. Within each pixel, two processes are happening
541 simultaneously: a certain amount of sediment erodes, and a certain amount of sediment accumulates. To
542 estimate the sediment redistribution for each pixel of each model run, we estimate which of these processes
543 dominated. Positive pixel values thus mean, bioturbation enhanced sediment accumulation, negative
544 pixel values mean, bioturbation enhanced sediment erosion. We tested the following environmental
545 parameters: mound density, vegetation cover, elevation, slope, aspect, TRI, TPI, curvature and
546 connectivity and wetness index. The model performance was evaluated by the percentage of explained
547 data variance. We analyzed the impact of environmental parameters within 1-meter and within 10-meter
548 distance from the burrows.

549

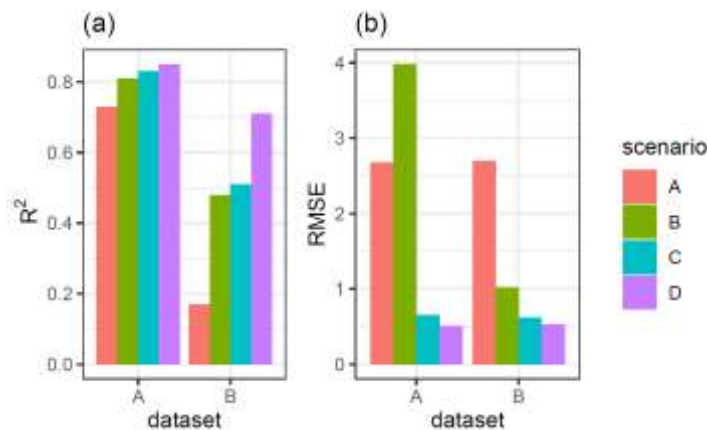
550 4 Results

551 4.1 Model sensitivity test and accuracy

552 Parameters which significantly influenced the model output were precipitation, slope, vegetation cover,
 553 surface roughness, silt content and water content (Table A2). There was correlation between some of
 554 the spatial model parameters (Fig. A10), especially between the initial and saturated water content;
 555 between water content and vegetation cover; and between clay content and field capacity. However, a
 556 high correlation between spatial parameters does not mean that these parameters impact the sediment
 557 redistribution in a similar way.

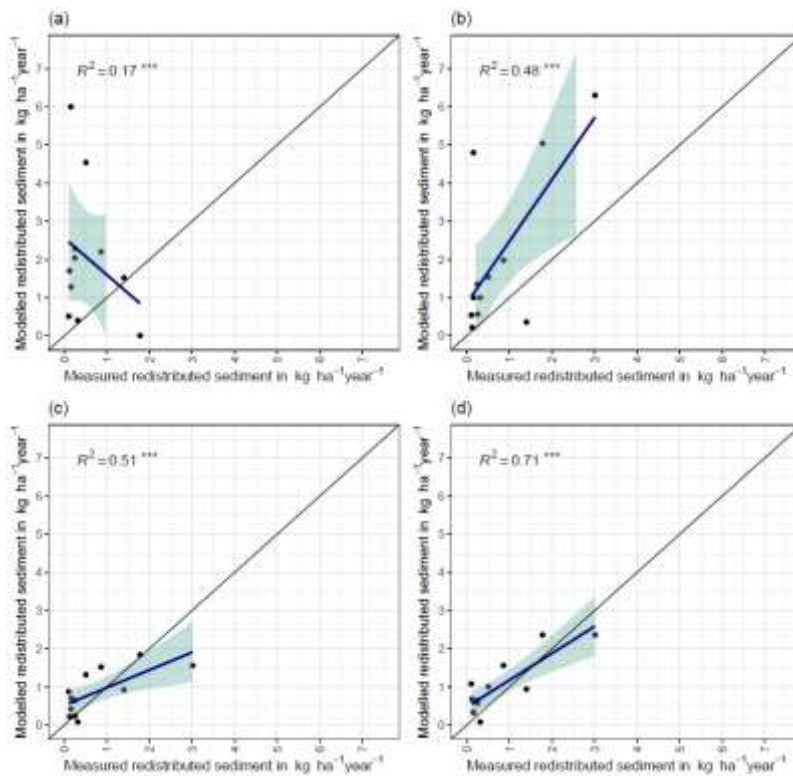
558 We quantified the model performance by comparing the modelled and measured sediment
 559 redistribution. The performance varied depending on the burrow inclusion (Figure 4 and 5). The
 560 performance of the model without any bioturbation was lower ($R^2 = 0.73$, RMSE = 1.50, MSE = 2.27),
 561 as when burrow entrances ($R^2 = 0.81$, RMSE = 1.34, MSE = 1.16) or mounds ($R^2 = 0.83$, RMSE = 1.10,
 562 MSE = 1.22) were included. The model had the highest performance when entire burrows were included
 563 ($R^2 = 0.85$, RMSE = 1.01, MSE = 1.01). However, as the scatterplots showed, the model performance
 564 seemed to be determined strongly by one measurement (Fig. 5). For this reason, we calculated the
 565 metrics without this measurement (Fig. A2). The model without any burrows ($R^2 = 0.17$, RMSE = 1.18,
 566 MSE = 1.39) in this case performed much lower than models with burrows. The model performance
 567 continuously strongly increased when burrow entrances ($R^2 = 0.48$, RMSE = 0.61, MSE = 0.78), or
 568 mounds ($R^2 = 0.51$, RMSE = 0.75, MSE = 0.57) were included. The model with whole burrows reached
 569 the highest performance ($R^2 = 0.71$, RMSE = 0.63, MSE = 0.39). When we compare the modelled
 570 redistribution to the sediment redistribution estimated using Time-of-Flight cameras in Grigusova et al.
 571 (2022), the differences appear to be minor ($R^2 = 0.62$, RMSE = 0.12, MSE = 0.35).

572



573
 574 **Figure 4.** R^2 and RMSE of the Morgan-Morgan-Finney soil erosion model. For dataset A, we compared
 575 the amount of sediment collected in all sediment fences with the modelled eroded sediment (see Fig.
 576 A3). For dataset B, we removed one measurement, as the R^2 seemed to be defined by this
 577 measurement (see Fig. A4). For Scenario A, we did not include any burrows into the model. For scenario
 578 B, we included burrow entrances and for scenario C, we included mounds. For scenario D, we included
 579 whole burrows into the model. The adjustments made to include entrances, mounds and burrows into
 580 the model are described in section 3.5.2.

581



582

583

584 **Figure 5.** Measured and modelled redistributed sediment without an outlier. (a) Model without
 585 bioturbation. (b) Model with entrances. (c) Model with mounds. (d) model with burrows.

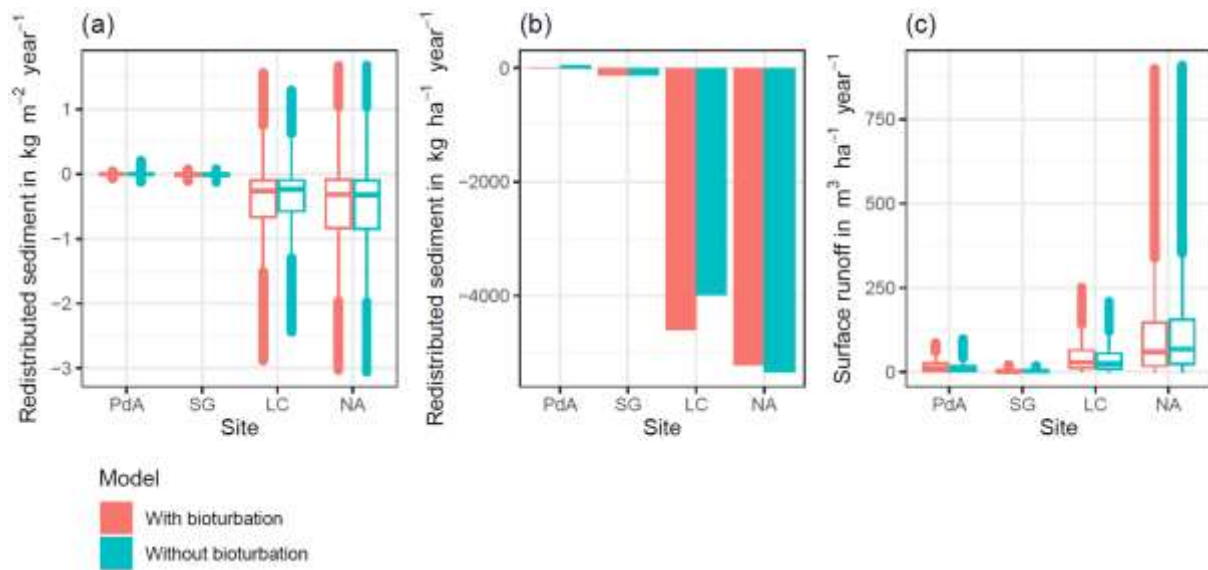
586

587 **4.2 Model output: Surface runoff and sediment redistribution**

588 Hillslope catchment – wide sediment redistribution (1 ha resolution) was the highest in humid NA,
 589 followed by Mediterranean LC, semi-arid SG and arid PdA (Fig. 6a, 6b, 8). In NA, LC and SG, the erosion
 590 processes dominated, while in PdA, more sediment accumulated than eroded. **The impact of burrows**
 591 **on sediment redistribution was significant in arid PdA, semi-arid SG and Mediterranean LC. Burrows**
 592 **increased sediment redistribution by 137.8 % ±16.4 % in arid PdA (3.53 kg ha⁻¹ year⁻¹ vs. 48.79 kg ha⁻¹**
 593 **year⁻¹), by 6.5 % ±0.7 % in semi-arid SG (129.16 kg ha⁻¹ year⁻¹ vs. 122.05 kg ha⁻¹ year⁻¹) and by 15.6 %**
 594 **±0.3 % in Mediterranean LC (4602.69 kg ha⁻¹ year⁻¹ vs. 3980.96 kg ha⁻¹ year⁻¹). Overall, bioturbation**
 595 **increased sediment accumulation in the arid zone (as the magnitude of the sediment excavation by the**
 596 **animal exceeded sediment erosion which occurs during rainfall events), but increased sediment erosion**
 597 **in semi-arid and Mediterranean climate (where animal burrowing activity and rainfall is present). The**
 598 **largest impact was found under Mediterranean conditions. We found no significant effect on**
 599 **redistribution in the humid zone (Figure 7). However, impact of bioturbation varied throughout the**
 600 **hillslope catchment (Figure 7, 8 and 9) – it depended on a specific context if bioturbation supports**
 601 **sediment erosion or accumulation.**

602 Surface runoff was the highest in humid NA, followed by Mediterranean LC, arid PdA and semi-arid SG
 603 (Figure 6c). The impact of burrows on surface runoff was significant in all climate zones. Burrows
 604 increased surface runoff in PdA by 34 %, in SG by 40% and in LC by 4.1 %; and decreased surface
 605 runoff by 5.9 % in NA. Hillslope catchment-wide maps are shown in Fig. A6-A8.

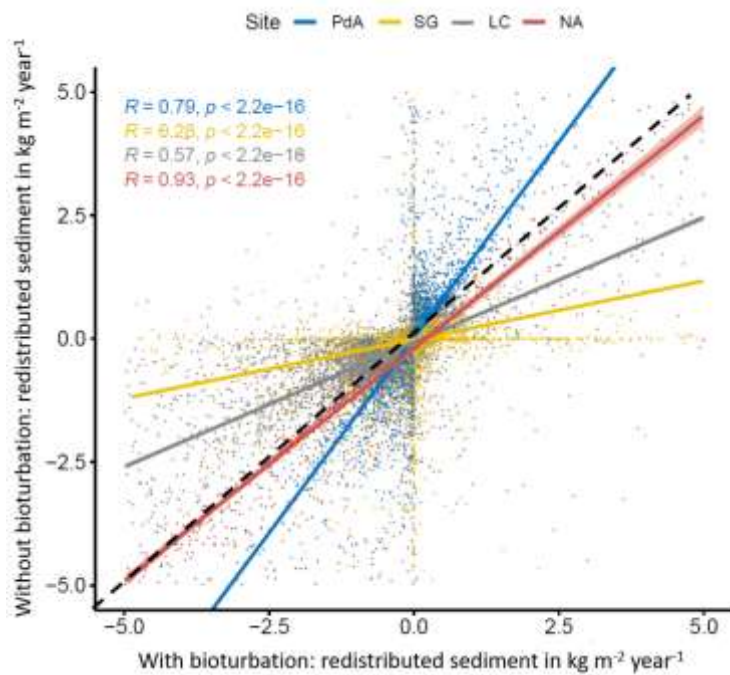
606



607
608

609 **Figure 6.** Summary of model outputs across the climate gradient. PdA is arid Pan de Azúcar, SG is
610 semi-arid Santa Gracia, LC is Mediterranean La Campana, NA is humid Nahuelbuta. Graphs (a) and
611 (b) show the modelled sediment redistribution. Positive values indicate sediment accumulation; negative
612 values indicate sediment erosion, in(a) sediment redistribution is shown on a pixel scale in $\text{kg m}^{-2} \text{ year}^{-1}$,
613 while in(b) sediment redistribution is shown on the hillslope catchment scale in $\text{kg ha}^{-1} \text{ year}^{-1}$. The
614 impact of bioturbation on sediment redistribution was estimated by a t-test and was significant in three
615 sites: PdA^{***}, SG^{**} and LC^{***}. Bioturbation increased sediment redistribution by 137.8 % in PdA, by 6.5
616 % in SG and by 15.6 % in LC. For hillslope catchment-wide maps see Fig. A6-A8. Graph (c) represents
617 the modelled surface runoff on the hillslope catchment scale in $\text{m}^3 \text{ ha}^{-1} \text{ year}^{-1}$. The impact of bioturbation
618 on surface runoff was estimated by a t-test and was significant at all sites. Bioturbation increased surface
619 runoff in PdA by 34 %, in SG by 40 % and in LC by 4.1 %; and decreased surface runoff by 5.9 % in
620 NA. For hillslope catchment-wide maps see Fig. A6.

621



622

623 **Figure 7.** Comparison of the model outputs with and without bioturbation of each pixel (0.5 m) in all

624 study sites. The x-axis shows the output of the model with bioturbation, the y-axis the model output

625 without bioturbation. PdA is arid Pan de Azúcar, SG is semi-arid Santa Gracia, LC is Mediterranean La

626 Campana, NA is humid Nahuelbuta. Points represent single pixel values; lines show linear regressions

627 for the sites. The lower R, the higher the impact of burrows on sediment redistribution at the resolution

628 of 0.5 m. The black dashed line symbolizes a perfect correlation – along this line the bioturbation would

629 have no effect on sediment redistribution. Bioturbation lead to more accumulation if the regression line

630 representing results from a particular climate zone is steeper than the perfect correlation line.

631 Bioturbation lead to more erosion if the regression line representing results from a particular climate

632 zone is flatter than the perfect correlation line. Bioturbation increases sediment accumulation in arid

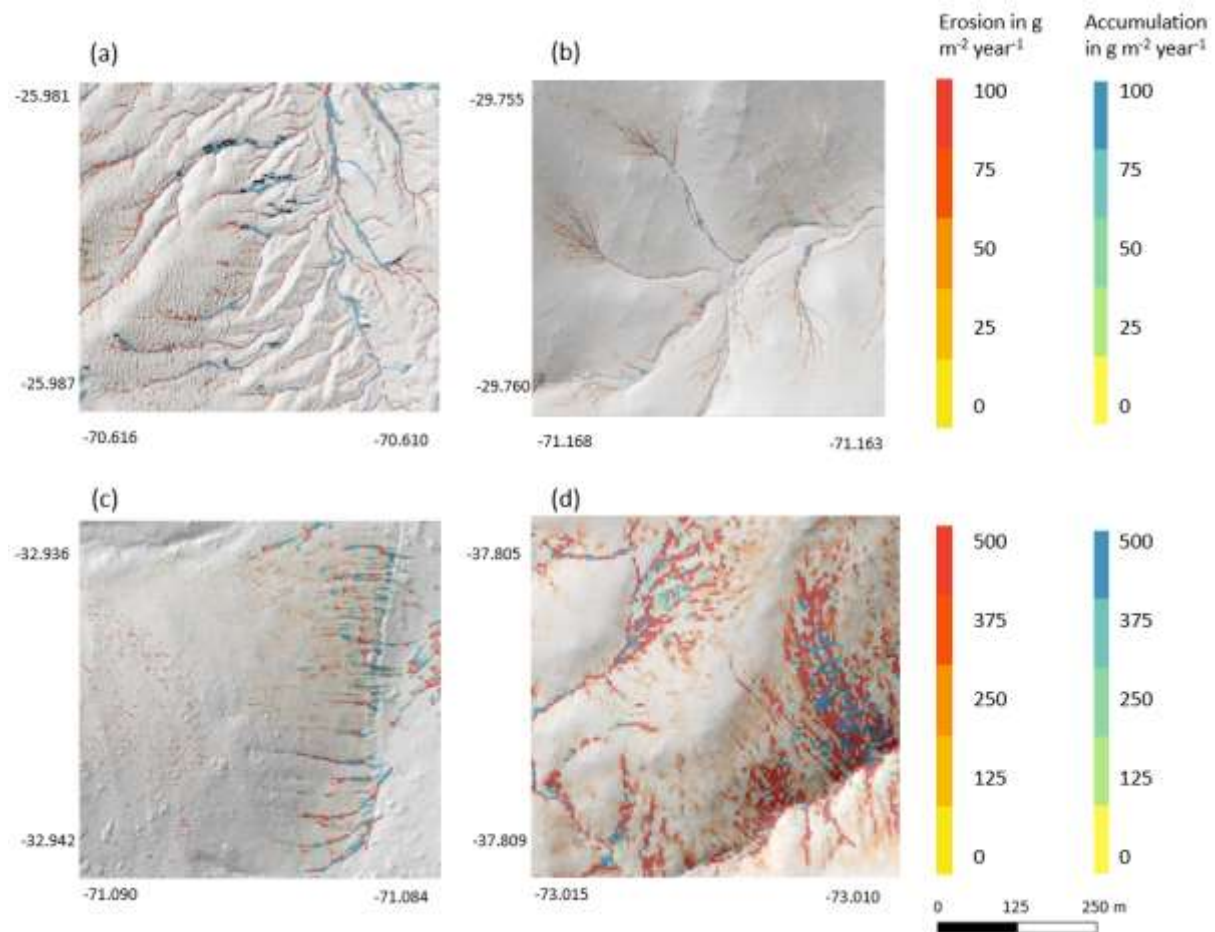
633 PdA (through the high burrowing rate, more sediment is accumulated on the surface than eroded during

634 rainfall events). Bioturbation increases sediment erosion in semi-arid SG and Mediterranean LC.

635 Absolutely, the highest impact on sediment redistribution is in the Mediterranean climate zone. The

636 lowest impact is in the humid zone.

637



638
 639 **Figure 8.** Hillslope catchment-wide predicted sediment redistribution. Colours indicate sediment
 640 redistribution. Grey shadows indicate the hill shading calculated from LiDAR data. (a) Pan de Azúcar,
 641 (b) Santa Gracia, (c) La Campana, (d) Nahuelbuta.

642

643 **4.3 Role of continuous burrowing activity on sediment redistribution**

644 We included the excavation of the sediment by **the animal** itself into the model. **The density of burrows**
 645 **was the highest in arid PdA, then Mediterranean LC, semi-arid SG and the lowest in humid NA. Burrows**
 646 **were mostly distributed within groups of several burrows in Mediterranean LC and semi-arid SG, while**
 647 **they were more evenly distributed in arid PdA and humid NA. The burrows were of largest size in**
 648 **Mediterranean LC, followed by arid PdA, semi-arid SG and humid NA. Similarly, the highest volume of**
 649 **excavated sediment at the beginning of the modelling period was in Mediterranean LC and arid PdA.**
 650 **The volume of excavated sediment during the burrow reconstruction after rainfall events was the highest**
 651 **in humid NA, followed by Mediterranean LC, semi-arid SG and arid PdA. The percentage of sediment**
 652 **excavated by the animal to sediment redistributed during rainfall events was 128 % in PdA, 24 % in SG,**
 653 **33.5 % in LC and 5.6 % in NA.**

654

655 **Table 2.** Impact of animal bioturbation activity on overall sediment redistribution on various scales. The
 656 bioturbation activity was estimated using Time-of-Flight based cameras in Grigusova et al. 2022. This
 657 study showed that animals reconstruct their burrows after each rainfall events. During this process, 10
 658 % of the overall sediment burrow volume is relocated from within the burrow to the surface. We

659 integrated this process into our model and calculated the percentage of newly excavated sediment by
 660 the animals to the amount of sediment which was redistributed during rainfalls for the period of one year.

Parameter	Units	PdA	SG	LC	NA
Burrow density	ha ⁻¹	91.35	71.50	84.36	13.30
Burrow aggregations	%	24	62	73	5
Burrow size	m ³	0.015	0.012	0.047	0.008
Sediment at the surface at the start of modelling	m ³ ha ⁻¹	1.35	0.88	4.11	0.10
Sediment excavated after each rainfall	m ³ ha ⁻¹	0.07	0.04	0.22	0.01
Number of rainfall events	year ⁻¹	3	7	16	137
Sediment excavated by the animal after the rain	m ³ ha ⁻¹ year ⁻¹	0.21	0.28	3.52	0.69
Sediment redistributed due to rainfall	m ³ ha ⁻¹ year ⁻¹	0.44	1.17	10.51	12.21
Excavated sediment to redistributed sediment	%	47	24	33.5	5.6

661

662 4.4 Role of adjacent environment

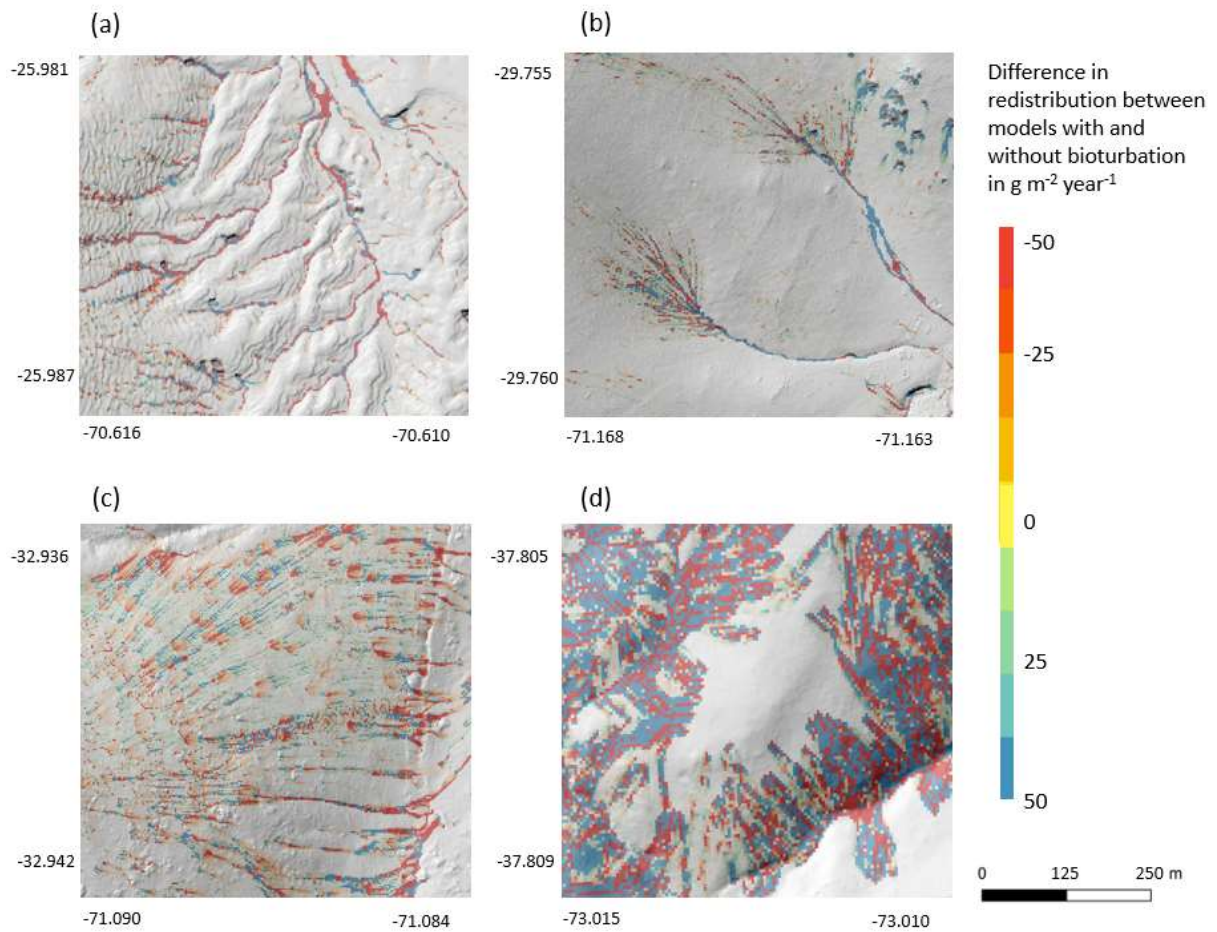
663 We subtracted the output of the model with included burrows from the output of the model without
 664 burrows (Figure A8). Although, the burrows on average enhanced sediment erosion on the hillslope
 665 catchment – scale, the high-resolution maps unveiled that burrows enhance sediment erosion within
 666 some pixels while they rather increased sediment accumulation within others.

667 The amount of data variance explained by the GAM models (see section 3.6.) differed between models
 668 (Table A3). Models estimating the impact of environmental parameters on sediment redistribution within
 669 1-meter distance from the burrows, explained 3.84 % of variance in PdA, 37.1 % in SG, 46 % in LC and
 670 42. % in NA. Models estimating the impact of environmental parameters on sediment redistribution
 671 within 10-meter distance from the burrows, explained 1.99 % of variance in PdA, 12.8 % in SG, 52 % in
 672 LC and 72.9 % in NA. The parameters selected for SG were slope, roughness, curvature, TRI and NDVI.
 673 Parameters selected for LC were elevation, slope, NDVI, sinks and roughness. Parameters selected for
 674 NA were elevation, slope, aspect, TRI, sinks and roughness (Figure 10).

675 Bioturbation strongly increased sediment redistribution (erosion and accumulation) at high values of
 676 elevation, slope, surface roughness TRI, sinks and topographic wetness index, at the middle values of
 677 elevation and aspect, and at low values of profile curvature and NDVI. From these parameters,
 678 bioturbation increased sediment erosion at high and middle values of elevation, at high values of slope,
 679 sinks and TRI, and at low values of profile curvature. Bioturbation increased sediment accumulation at
 680 high values of surface roughness and topographic wetness index and at low values of NDVI (Fig. A3 –
 681 A8).

682 Bioturbation somewhat enhanced sediment erosion at medium values of surface roughness, NDVI and
 683 sinks, and at low values of topographic wetness index. Bioturbation somewhat increased sediment
 684 accumulation at low values of slope and TRI, at low and medium values of elevation and at high values
 685 of profile curvature.

686



687

688

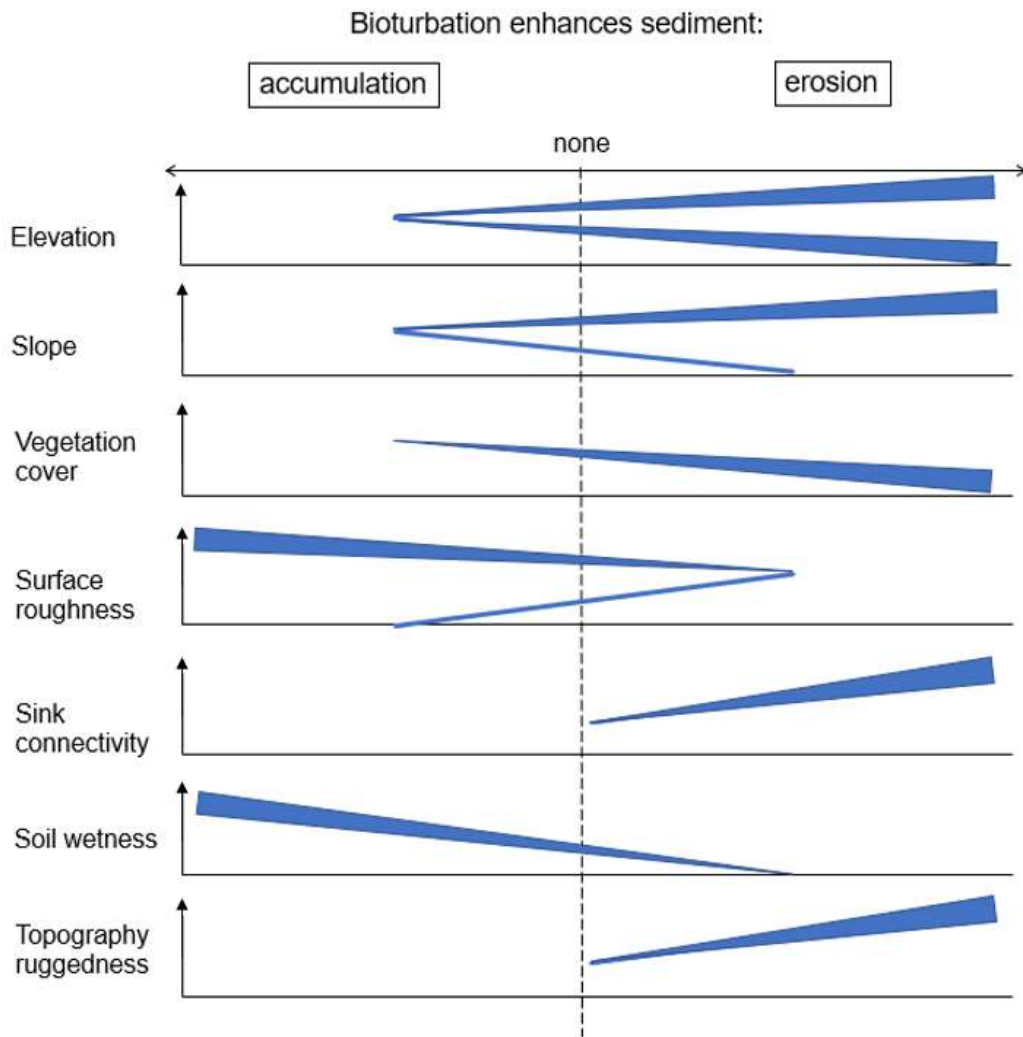
689

690

691

692

Figure 9. Hillslope catchment-wide impact of bioturbation on sediment redistribution. Colour indicates the impact. Positive values indicate bioturbation enhanced sediment accumulation, negative values indicate bioturbation enhanced sediment erosion. Grey shadows indicate the hill shading calculated from LIDAR data. (a) Pan de Azúcar, (b) Santa Gracia, (c) La Campana, (d) Nahuelbuta.



693
 694 **Figure 10.** This figure is a conceptual summary of the detailed results from figures A3 – A8. Bioturbation
 695 increases erosion or accumulation depending on the values of environmental parameters. The
 696 dependencies are the same for all climate zones. The figure is the conceptual summary for all climate
 697 zones, therefore, there are no values stated on the x- and y-axes. The x-axis shows if bioturbation
 698 increases erosion or accumulation. The y-axis are environmental parameters. Line thicknesses indicate
 699 the magnitude of impact. Please note that bioturbation has no impact on sediment redistribution in
 700 regions with low sink connectivity and topographic ruggedness. The relationship between the values of
 701 environmental parameters and the impact of bioturbation is not linear: Bioturbation can have the same
 702 impact on sediment redistribution at high or low values of an environmental parameter, but a contrasting
 703 impact at middle values of this parameter (as in this case for elevation, slope or surface roughness).

704

705 5. Discussion

706 5.1 The inclusion of bioturbation increases model performance

707 Overall, our DMMF model including bioturbation performed much better than the model without
 708 bioturbation. The DMMF model without bioturbation performed worse (RMSE of $1.18 \text{ kg ha}^{-1} \text{ year}^{-1}$ and
 709 R^2 of 0.17) than the model with bioturbation (RMSE was $0.63 \text{ kg ha}^{-1} \text{ year}^{-1}$ and R^2 was 0.71).

710 We hence argue that the higher accuracy of our model can be explained with the inclusion of
 711 bioturbation. This is confirmed by the fact that our model run without bioturbation performed similarly to

712 previously run models without bioturbation: In earlier studies, the accuracy of the MMF model reached
713 an RMSE in between 4.9 and 8.2 kg ha⁻¹ year⁻¹, with an estimated R² of in between 0.21 and 0.57 (Jong
714 et al., 1999; Vigiak et al., 2005; López-Vicente et al., 2008; Vieira et al., 2014; Choi et al., 2017).
715 However, we acknowledge that previous studies were all conducted in more temperate climate zones.
716 To be able to compare our results with previous studies, we calculated the model performance
717 considering solely the Mediterranean and humid climate zone, which are more similar in climate to the
718 more temperate locations of previous studies. The performance of the model was still high (R² = 0.72,
719 RMSE = 0.45 kg ha⁻¹ year⁻¹), confirming the conclusion that bioturbation increased model performance.
720 We compared the modelled impact of bioturbation on sediment redistribution with the impact of
721 bioturbation estimated in previous studies. In the humid zone, our model predicted an erosion up to 3.5
722 kg m⁻² year⁻¹. This estimation is in line with erosion rates established by in-situ measurements in other
723 studies conducted in a more humid climate zone (between 1.5 kg m⁻² year⁻¹ and 3.7 kg m⁻² year⁻¹) (Black
724 and Montgomery, 1991; Yoo and Mudd, 2008; Yoo et al., 2005; Rutin, 1996). This also confirms the
725 reliability of our approach. Previous authors estimated the impacts using rainfall simulators, erosion pins
726 or splash boards. The measurements were conducted for a time period between 3 months and 3 years
727 and the sites were revisited for each estimation. We do not compare our results with studies which
728 previously applied models to estimate impacts of bioturbation, as, to our knowledge, none of the
729 previous studies integrated vertebrate burrow structures into a soil erosion model and ran the model on
730 a daily basis.

731

732 **5.2 The relevance of bioturbation for sediment redistribution depends on the environmental** 733 **context**

734 On the hillslope catchment scale (1 ha), our study finds that bioturbation increases erosion in semi-arid
735 and Mediterranean zone, accumulation in the arid zone and has no impact within the humid zone (Figure
736 6b). In contrast, bioturbation increases both, erosion, and accumulation, on the plot scale (1 m²) (Figure
737 6a). On this scale, in the arid and semi-arid zone, sediment erosion and accumulation were predicted to
738 be about equal (erosion and accumulation both up to 0.1 kg m⁻² year⁻¹ in the arid zone, and erosion and
739 accumulation both up to 0.2 kg m⁻² year⁻¹ in the semi-arid zone (see Figure 6a)). Bioturbation marginally
740 increased erosion and decreased accumulation in the semi-arid zone but reduced by twofold
741 accumulation in the arid zone. In contrast, in the Mediterranean and humid zone, erosion was predicted
742 to be almost double when compared to accumulation (predicted erosion up to 2.5 kg m⁻² year⁻¹, and
743 accumulation up to 1.4 kg m⁻² year⁻¹). Inclusion of bioturbation increased erosion up to 3 kg m⁻² year⁻¹,
744 and accumulation up to 1.6 kg m⁻² year⁻¹ in the Mediterranean zone, while it had no significant effect in
745 the humid zone. We argue that sediment redistribution due to bioturbation is heavily influenced by meso-
746 topographic structures which determine the flow path of surface runoff and influence the infiltration
747 processes. Due to this, the erosion and accumulation on the plots scale is heavier impacted by
748 bioturbation with increasing surface runoff.

749 Our study found an increase of erosion in the semi-arid and Mediterranean climate zone to be between
750 6.5 % and 15.6 % due to bioturbation. Previous studies found that already a small increase of erosion
751 has significant impacts on the whole hillslope catchment. A 10% increase in erosion rates over a 10-

752 year period can lead to significant changes in the landscape, including e.g. a 20-30% reduction in soil
753 thickness and an increase in sediment transport in nearby rivers (Kuhn 2016).

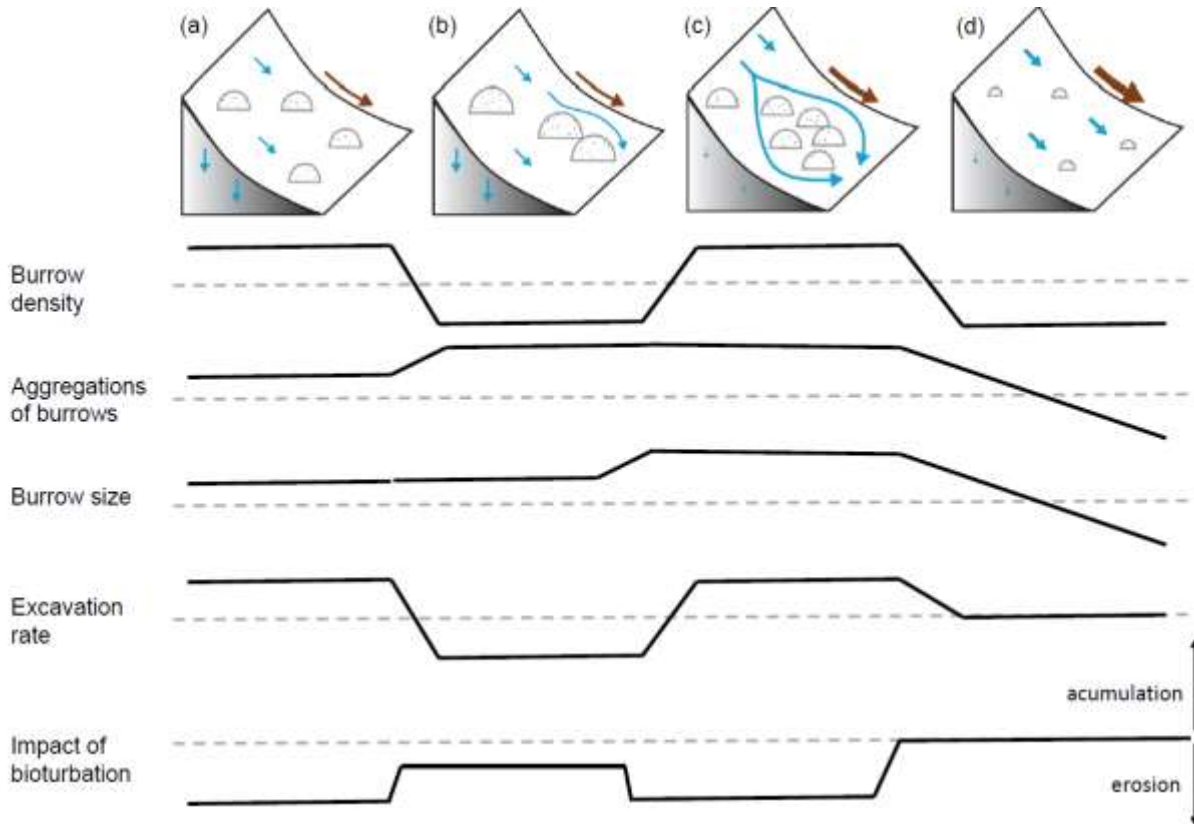
754 According to our analysis, bioturbation increases erosion or accumulation of sediment mostly based on
755 an interplay between topographic structures elevation, slope and TRI (Figure 10). Over all research
756 sites, this study found that bioturbation leads to an increase in surface erosion in areas where erosional
757 processes dominate (upper, and/or steeper slopes), and tends to increase sediment accumulation in
758 areas where sediment is naturally deposited, e.g. lower slopes or shallow depressions (Figure 10). This
759 finding is based on the fact that erosion in general is positively affected by slope, and negatively by
760 surface roughness and vegetation (Rodríguez-Caballero et al., 2012; Wang et al., 2013; Kirols et al.,
761 2015). Additionally, the redistribution of sediment is largely affected by topographic meso-/macroforms,
762 such as rills or cliffs. These can be quantified by topographic ruggedness index (TRI) which describes
763 the amount of elevation drop between adjacent cells of DEM (Wilson et al., 2007). At high values of this
764 index, we would therefore expect high erosion rate, due to concentrated runoff within the connected rills
765 or undisturbed flow of runoff from the cliffs downslope.

766 Our data show that one burrow provides up to 0.43 m³ of additional loose sediment at the surface (Table
767 2), while the surface roughness increases up to 200 % (Grigusova et al., 2022). When including burrows
768 into the model, at the slope values from 0 to 5 degrees, the presence of burrows had no impact on
769 sediment redistribution. From 5 degrees onwards it increased sediment erosion proportionally to the
770 slope of the hillside (an increased erosion from 0.4 g ha⁻¹ year⁻¹ in the semi-arid zone until up to 150 kg
771 ha⁻¹ year⁻¹ in the Mediterranean zone, Fig. A3 – A6). Similarly, at locations with elevation drops ranging
772 from 0 m until 0.2 m (lower TRI values), the presence of burrows had no impact. However, at locations
773 with elevation drops of 0.2 until 0.5 m (higher TRI values), bioturbation increases sediment erosion by
774 1.5 kg ha⁻¹ year⁻¹ (Fig. A3 – A8). Lastly, bioturbation proportionally increased accumulation when the
775 surface roughness values were above 0.5 (an increased accumulation from 0.2 g ha⁻¹ year⁻¹ in semi-arid
776 zone until 5000 kg ha⁻¹ year⁻¹ in the Mediterranean zone, Fig. A3 – A6).

777 We conclude that in locations with slope values over 5 degrees, or at locations with sudden drops in
778 elevation (high TRI), and connected rills, more sediment is eroding than accumulating. Here, additional
779 surface sediments generated by bioturbators provides more source material for erosion and thus
780 bioturbation increases sediment erosion at these locations (Figure 10 and 11). In contrast, at locations
781 with a slope below 5 degrees, where processes are dominantly controlled by surface roughness,
782 sediment accumulation caused by bioturbation increases proportionally when the surface roughness
783 has a value above 0.5. This is likely because burrows through their above-ground structures heavily
784 increase surface roughness (Grigusova et al., 2022), and hence the presence of bioturbating animals
785 leads to an increase in sediment accumulation.

786 Additionally, we hypothesize that it is not only the additional availability of sediment on the surface and
787 the topography of the vicinity which controls the contribution of bioturbation to sediment surface flux, but
788 also the spatial distribution of animal burrows. We interpret that in locations with high burrow
789 aggregation, surface flow might be redirected and centralized around the aggregates and thus increase
790 sediment erosion in the areas adjacent burrow aggregates (Figure 11). This mechanism could explain
791 why bioturbation promotes sediment erosion especially in the Mediterranean zone where burrows are

792 more aggregated. The relative role of burrow aggregation should be studied in detail and included in
 793 future studies.
 794



795
 796 **Figure 11.** Context dependency of sediment redistribution. (a) Pan de Azúcar, (b) Santa Gracia, (c) La
 797 Campana, and (d) Nahuelbuta. Brown arrows indicate the direction and magnitude of overall sediment
 798 redistribution within each climate zone. Blue arrows indicate the direction of flow (runoff vs. infiltration).
 799 Half-moons indicate the distribution and size of the burrows.

800
 801
 802 **6. Conclusion**

803 Our study found that the inclusion of vertebrate bioturbators' burrows into a soil erosion model
 804 significantly increases its reliability. Vertebrate bioturbators increase sediment accumulation in the arid
 805 climate zone, sediment erosion in the semi-arid and Mediterranean zone and have no impact on
 806 sediment redistribution in the humid. Our study furthermore shows that the impact of bioturbation heavily
 807 depends on the adjacent environmental parameters. The burrows increase sediment erosion at high
 808 and low values of elevation, at high values of slope, sink connectivity and topography ruggedness, and
 809 at low values of vegetation cover. The burrows increase accumulation at high values of surface
 810 roughness and soil wetness. This means that overall, on geological time scales, as burrowing animals
 811 increase both, erosion in steeper zones, and accumulation in areas with gentler slopes and higher
 812 roughness, hillslope relief should become faster equalised and overall, more flat. This tendency is most
 813 pronounced in the Mediterranean zone with high burrow density and excavation rates, as well as
 814 comparably high precipitation rates.

815
816 **Funding:** This study was funded by the German Research Foundation, DFG [grant numbers
817 BE1780/52-1, LA3521/1-1, FA 925/12-1, BR 1293-18-1], and is part of the DFG Priority Programme
818 SPP 1803: EarthShape: Earth Surface Shaping by Biota, sub-project “Effects of bioturbation on rates
819 of vertical and horizontal sediment and **nutrient fluxes**”.

820 **Institutional Review Board Statement:** Not applicable.

821 **Informed Consent Statement:** Not applicable.

822 **Acknowledgments:** We thank CONAF for the kind support provided during our field campaign.

823 **Competing interests:** There is no conflict of interest.

824 **Author contribution:** PG set up the model, analysed the data and wrote the manuscript draft; PG and
825 AL performed the measurements AL, JB, NF, RB, DK, PP, LP, CdR reviewed and edited the manuscript.

826 **Code/Data availability:** The estimated soil properties (DOI: 10.5678/wsrb-9f70), modelled sediment
827 redistribution (DOI: 10.5678/32wa-d179) and model code ([https://gitlab.uni-marburg.de/fb19/ag-](https://gitlab.uni-marburg.de/fb19/ag-bendix/model-sediment-redistribution-caused-by-bioturbating-animals)
828 [bendix/model-sediment-redistribution-caused-by-bioturbating-animals](https://gitlab.uni-marburg.de/fb19/ag-bendix/model-sediment-redistribution-caused-by-bioturbating-animals)) was published via LCRS data
829 **services**.

830 **Special Issue statement:** I would like to stress that the submission should be part of the Copernicus
831 special Issue (Earth surface shaping by biota (ESurf/BG/ESD/ESSD/SOIL inter-journal SI) initiated by
832 the EarthShape consortium.

833

834

835 burrows. The dashed line indicates the median value of each parameter for the first four parameters.

836

837 **Supplementary material**

838 **Table A1:** R² and RMSE of random forest models trained for the prediction of soil properties needed for
839 model parametrization. RMSE is root mean square error.

Variable	R ²	RMSE
Soil water content	0.80	0.05
Bulk density	0.60	0.22
Porosity	0.63	0.09
Silt	0.64	0.04
Middle silt	0.64	0.04
Sand	0.68	0.09
Middle sand	0.64	0.05
Organic components	0.77	0.05
Organic carbon	0.70	0.03

840

841 **Table A2.** Model sensitivity analysis. For the analysis, the minimum, maximum and mean value of each
842 parameter was calculated. The model was run for a hillslope catchment of 1km² with homogenous mean
843 parameters. Then, the minimum and maximum values of each parameter were tested. Each parameter
844 was stepwise changed to its minimum or maximum value while the remaining parameters stayed
845 homogenous. The significance of the parameter was estimated by a t-test conducted between the

846 erosion estimated by the model with homogenous mean parameters and the erosion estimated by the
 847 model with varying minimum and maximum parameter values. Only significant parameters are shown.

Parameter	mean value	min value	max value	mean erosion [kg m ⁻¹]	Min erosion [kg m ⁻¹]	Max erosion [kg m ⁻¹]	Erosion [kg m ⁻¹]
Precipitation [mm rainfall event ⁻¹]	19.9	0.2	65.6	0.07	0	4.1	
clay content [%]	10.61	3.87	34.64	0.07	0.07	0.07	
silt content [%]	38.49	13.32	59.59	0.07	0.04	0.11	
sand content [%]	47.04	24.13	79.17	0.07	0.07	0.07	
water content [%]	3.87	2.38	12.68	0.07	0.09	0.06	
roughness [-]	0.97	0	236.8	0.07	0.34	0.01	
vegetation [%]	79.54	50.38	92.48	0.07	0.01	0.004	
Slope of DEM [°]	18.2	0	89.78	0.07	0	inf.	

848

849

850 **Table A3.** Summary of GAM models. We analyzed the impact of parameters within a 1-meter and 10-
 851 meter distance from burrows. The Stars indicate p-values of the selected parameters. p*** < 0.001, p**
 852 < 0.01, p* < 0.05, p. < 0.1. One GAM model was run per parameter. Only results for models with an
 853 explained variance above 5 % are shown.

Parameters	Within 1 meter from burrows				Within 10 meters from burrows			
	PdA	SG	LC	NA	PdA	SG	LC	NA
Explained Variance	3.8 %	37 %	46 %	42 %	2.0 %	13 %	52 %	73 %
Burrow density	.				.			
Elevation			***	***	*		*	***
Slope		***					*	**
Aspect	.	**		*	*			.
Roughness		***					**	*

TPI								
TRI		**		**				
Plan curvature		.						.
Profile curv.		**	.					
NDVI			**			**		.
Sinks			*	***	*		*	
Wetness				**				
Flow direction								
Flow path								
Catchment		*			*			
Catchment slope		***		.				

854

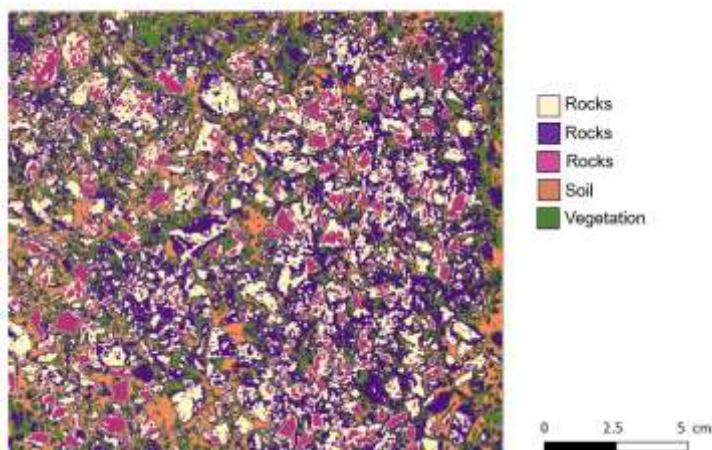
855 **Table A4.** Review of studies which integrated any kind of bioturbation into models. Previous models
856 integrated either benthic, invertebrate or single species of vertebrate bioturbators. Models applied
857 either described the vertical soil mixing or long-term landscape evolution models. None of the previous
858 studies included vertebrate burrows of bioturbators into an erosion model which would be capable to
859 capture the daily redistribution processes.

References	Bioturbators	Integrated processes	Targeted process	Model
Francois et al. 1997, Francois et al. 2002, Kadko and Heath 1984, Croix et al. 2002 and several others	Various benthic bioturbators	Equations describing soil mixing within a floodplain	Vertical soil mixing within a floodplain	Mathematical equations
Orvain et al. 2006, Román – Sánchez et al. 2019, Orvain 2005, Orvain 2003, Sanford 2008 and several others	Various invertebrates	Equations describing vertical soil mixing	Influence of vertical soil mixing on lateral redistribution	Mathematical equations
Gabet 2000	Pocket gophers	Equation describing diffusion caused by gopher bioturbation	Relief changes over 40 000 years, lateral redistribution	Landscape evolution
Gabet et al. 2014	Pocket gophers	Equations describing sediment accumulation caused by gophers	Relocation of sediment to create Mima mounds	Landscape evolution
Temme and Vanwallegem 2016	Not specified invertebrates	Bioturbation causes soil mixing between model layers. Mixing	Soil and landscape evolution	Landscape evolution

Vanwallegem et al. 2013		is proportional to depth in the profile, soil thickness, and soil carbon content, and layer distance		Landscape evolution
Yoo and Mudd 2008		Bioturbation is considered as the cause of colluvial transport. Colluvial fluxes are calculated as a function of soil thickness and slope gradient on sloping grounds		Landscape evolution
Pelletier et al. 2013		Vertical soil mixing. Rate increases linearly with aboveground biomass.	creep including abiotic and bioturbation-driven transport	Landscape evolution
Van der Meij et al. 2020		Vertical soil mixing. Rate depends on vegetation type.	Soil and landscape evolution	Landscape evolution
Our model	Vertebrates	The model includes burrow structure, adjusted soil properties and adjusted vegetation cover. Burrow distribution determined by machine learning.	Daily lateral sediment redistribution	Daily erosion model

860

861



862

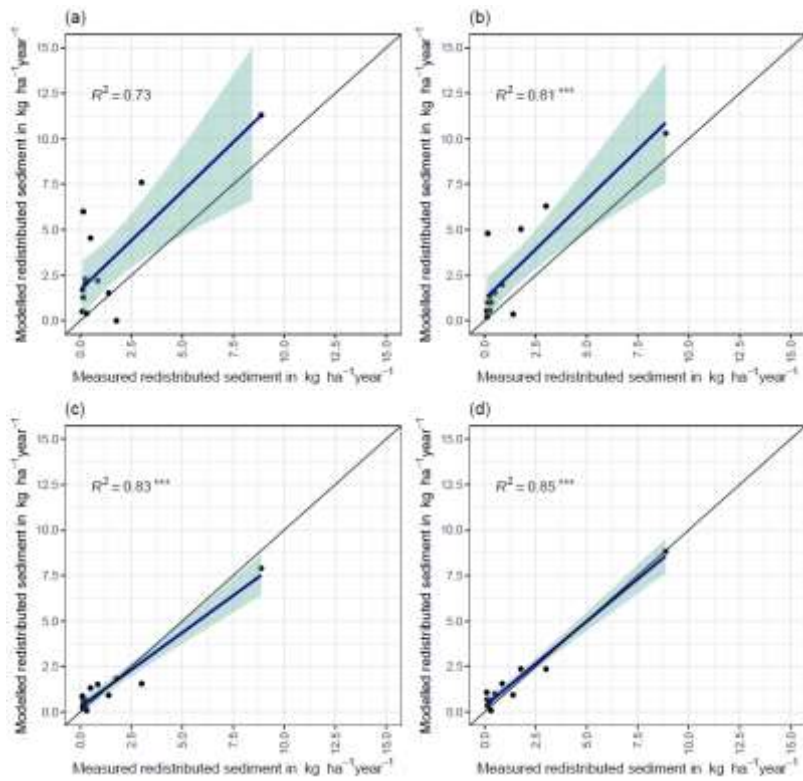
863 **Figure A1.** Example of the unsupervised k-means classification of the surface photo from La Campana.

864 Original photo was taken by Paulina Grigusova. The collection of in-situ data is explained in section 3.1.,

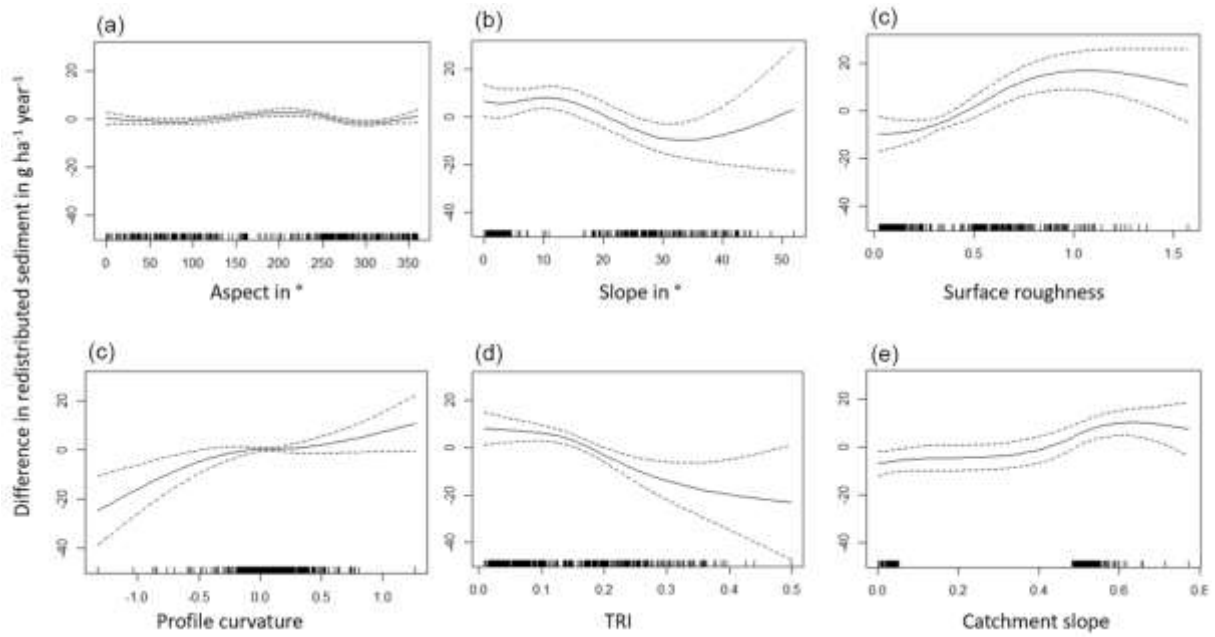
865 the estimation of soil properties in section 3.2. The image was classified into 5 classes using

866 unsupervised k-means classification; the land cover was then assigned manually. In some cases, like

867 in this case for rocks, multiple k-means classes stand for the same land cover. These were then unified
868 to the class "rocks".
869
870

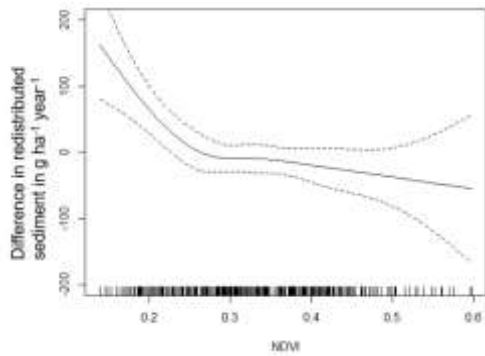


871
872 **Figure A2.** Measured and modelled redistributed sediment for different scenarios. (a) Model without
873 bioturbation. (b) Model with entrances. (c) Model with mounds. (d) model with burrows.
874
875
876
877
878



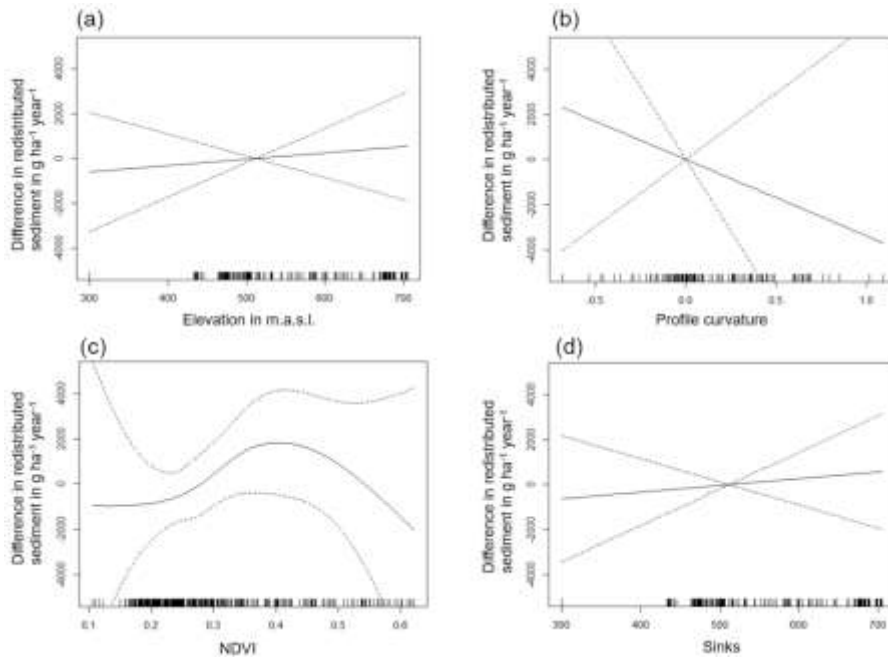
879
880
881
882
883
884

Figure A3. Environmental parameters influencing impact of bioturbation on sediment redistribution in Santa Gracia within 1-meter distance from burrows. Positive values indicate bioturbation enhances sediment accumulation at the respective parameter values, negative values indicate bioturbation enhances sediment erosion at the respective parameter values.

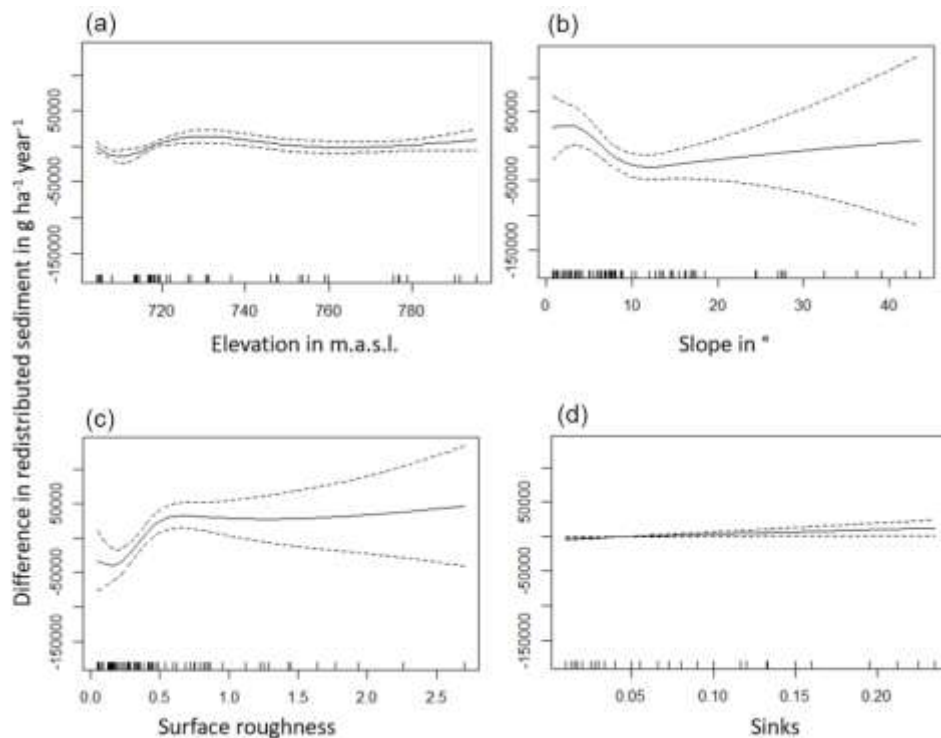


885
886
887
888
889
890
891

Figure A4. Environmental parameters influencing impact of bioturbation on sediment redistribution in Santa Gracia within 10-meter distance from burrows. Positive values indicate bioturbation enhances sediment accumulation at the respective parameter values, negative values indicate bioturbation enhances sediment erosion at the respective parameter values.

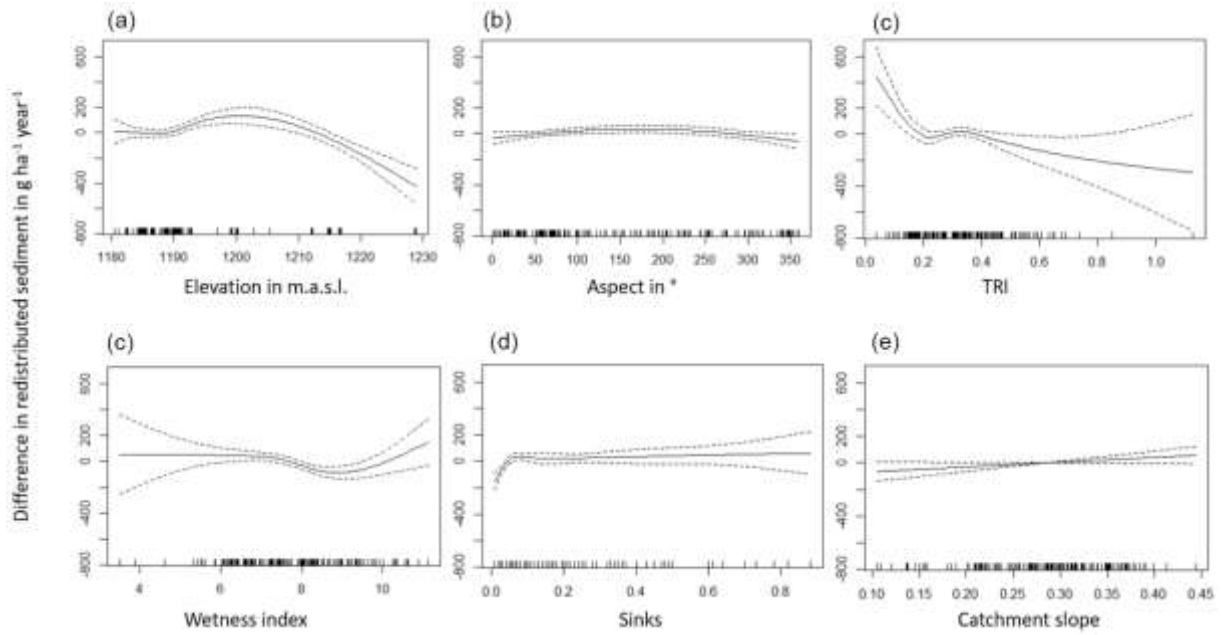


892
 893 **Figure A5.** Environmental parameters influencing impact of bioturbation on sediment redistribution in
 894 La Campana within 1-meter distance from burrows. Positive values indicate bioturbation enhances
 895 sediment accumulation at the respective parameter values, negative values indicate bioturbation
 896 enhances sediment erosion at the respective parameter values.
 897



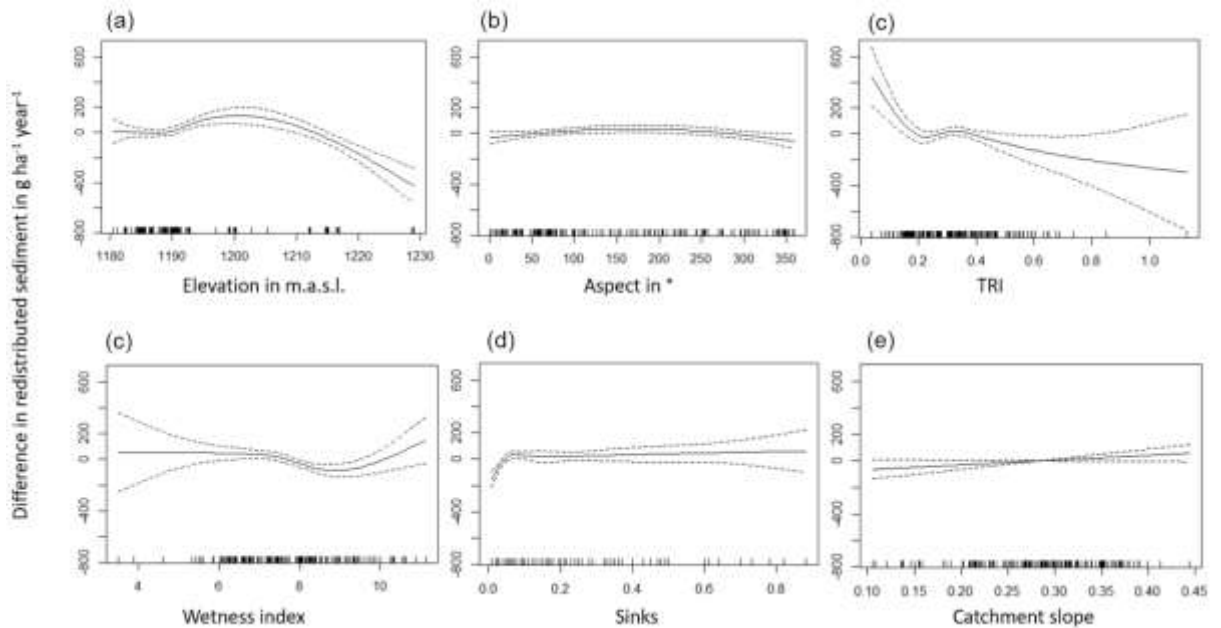
898
 899 **Figure A6.** Environmental parameters influencing impact of bioturbation on sediment redistribution in
 900 La Campana within 10-meter distance from burrows. Positive values indicate bioturbation enhances
 901 sediment accumulation at the respective parameter values, negative values indicate bioturbation
 902 enhances sediment erosion at the respective parameter values.
 903

904



905

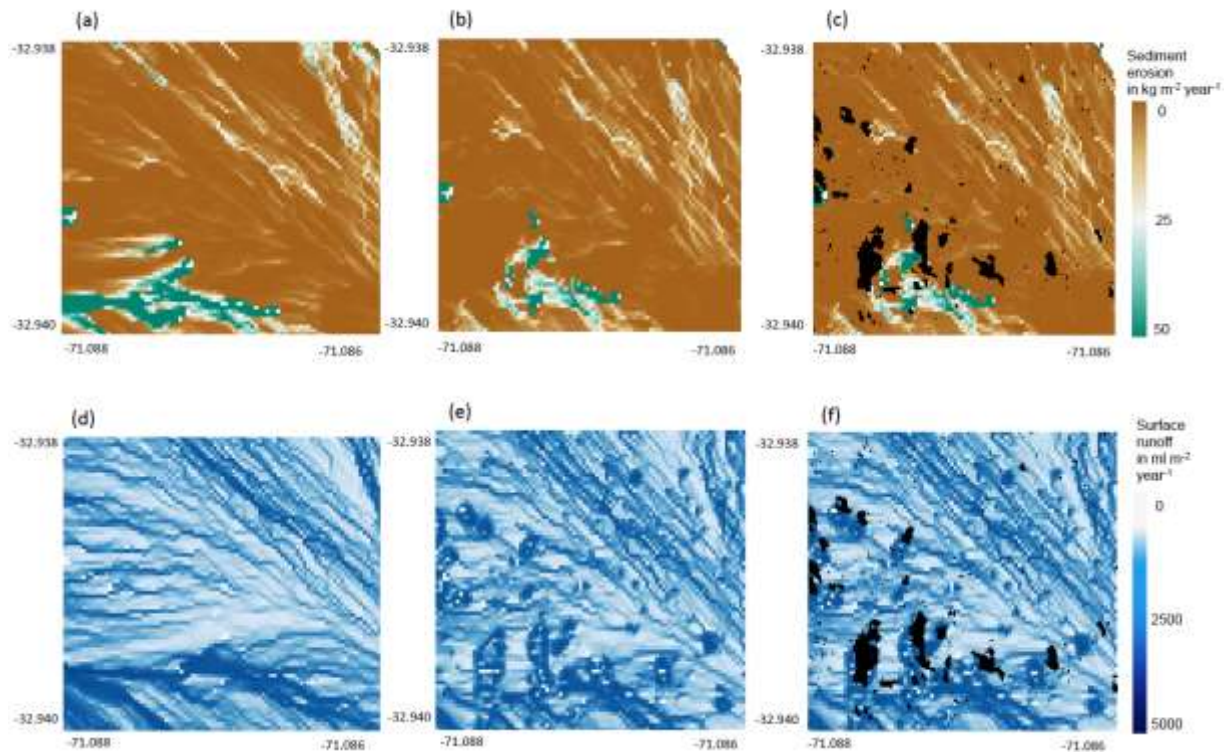
906 **Figure A7.** Environmental parameters influencing impact of bioturbation on sediment redistribution in
907 Nahuelbuta 1-meter distance from burrows. Positive values indicate bioturbation enhances sediment
908 accumulation at the respective parameter values, negative values indicate bioturbation enhances
909 sediment erosion at the respective parameter values.



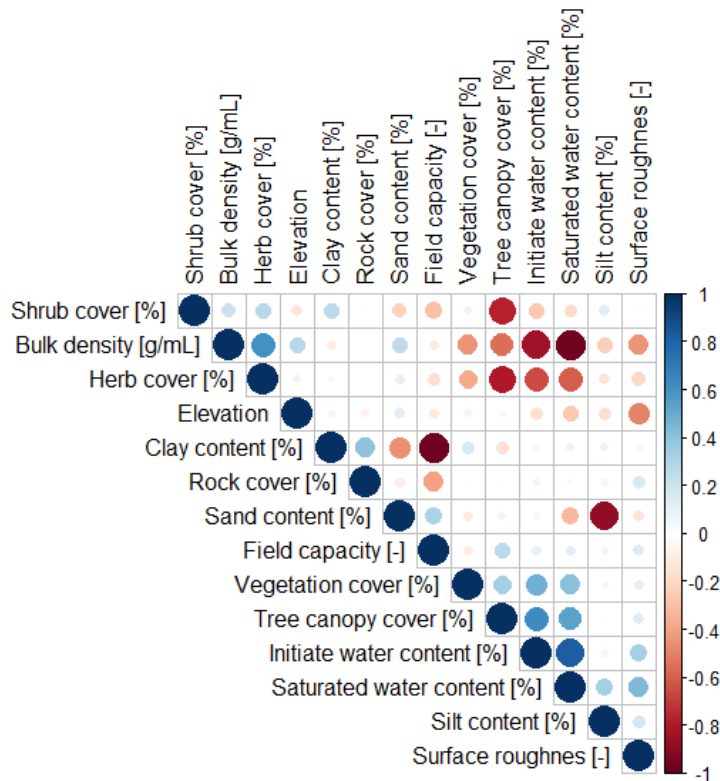
910

911 **Figure A8.** Environmental parameters influencing impact of bioturbation on sediment redistribution in
912 Nahuelbuta 10-meter distance from burrows. Positive values indicate bioturbation enhances sediment
913 accumulation at the respective parameter values, negative values indicate bioturbation enhances
914 sediment erosion at the respective parameter values.

915



916
 917 **Figure A9.** Burrow aggregation concentrates the runoff and increases erosion. Example for the north-
 918 facing hillside in Mediterranean La Campana for the time period of one year. (a) Sediment erosion as
 919 estimated by model without bioturbation. (b) Sediment erosion as estimated by model with bioturbation.
 920 (c) Sediment erosion as estimated by model with bioturbation with predicted burrow locations. (d)
 921 Surface runoff as estimated by model without bioturbation. (e) Surface runoff as estimated by model
 922 with bioturbation. (f) Surface runoff as estimated by model including bioturbation and predicted burrow
 923 locations. Black colour indicates, at least one burrow was located within this pixel. Four neighbouring
 924 pixels which contain a burrow form a burrow aggregation.
 925



926
927
928
929

Figure A10. Correlation matrix between the model input parameters.

930 References

- 931 Anderson, R. S., Rajaram, H., and Anderson, S. P.: Climate driven coevolution of weathering profiles and
932 hillslope topography generates dramatic differences in critical zone architecture, *Hydrol. Process.*, 33, 4–19,
933 <https://doi.org/10.1002/hyp.13307>, 2019.
- 934 Beasley, D. B., Huggins, L. F., and Monke, E. J.: ANSWERS: A Model for Watershed Planning, *Transactions of the*
935 *ASAE*, 23, 938–944, <https://doi.org/10.13031/2013.34692>, 1980.
- 936 Bernhard, N., Moskwa, L.-M., Schmidt, K., Oeser, R. A., Aburto, F., Bader, M. Y., Baumann, K., Blanckenburg, F.
937 von, Boy, J., van den Brink, L., Brucker, E., Büdel, B., Canessa, R., Dippold, M. A., Ehlers, T. A., Fuentes, J. P.,
938 Godoy, R., Jung, P., Karsten, U., Köster, M., Kuzyakov, Y., Leinweber, P., Neidhardt, H., Matus, F., Mueller,
939 C. W., Oelmann, Y., Oses, R., Osses, P., Paulino, L., Samolov, E., Schaller, M., Schmid, M., Spielvogel, S.,
940 Spohn, M., Stock, S., Stroncik, N., Tielbörger, K., Übernickel, K., Scholten, T., Seguel, O., Wagner, D., and
941 Kühn, P.: Pedogenic and microbial interrelations to regional climate and local topography: New insights from
942 a climate gradient (arid to humid) along the Coastal Cordillera of Chile, *CATENA*, 170, 335–355,
943 <https://doi.org/10.1016/j.catena.2018.06.018>, 2018.
- 944 Beven, K. J. and Kirkby, M. J.: A physically based, variable contributing area model of basin hydrology / Un
945 modèle à base physique de zone d'appel variable de l'hydrologie du bassin versant, *Hydrological Sciences*
946 *Bulletin*, 24, 43–69, <https://doi.org/10.1080/02626667909491834>, 1979.
- 947 Black, T. A. and Montgomery, D. R.: Sediment transport by burrowing mammals, Marin County, California, *Earth*
948 *Surf. Process. Landforms*, 16, 163–172, <https://doi.org/10.1002/esp.3290160207>, 1991.
- 949 Boudreau, B. P.: Mathematics of tracer mixing in sediments; I, Spatially-dependent, diffusive mixing, *American*
950 *Journal of Science*, 286, 161–198, <https://doi.org/10.2475/ajs.286.3.161>, 1986.

- 951 Boudreau, B. P.: The diffusion and telegraph equations in diagenetic modelling, *Geochimica et Cosmochimica*
952 *Acta*, 53, 1857–1866, [https://doi.org/10.1016/0016-7037\(89\)90306-2](https://doi.org/10.1016/0016-7037(89)90306-2), 1989.
- 953 Braun, J., Mercier, J., Guillocheau, F., and Robin, C.: A simple model for regolith formation by chemical
954 weathering, *J. Geophys. Res. Earth Surf.*, 121, 2140–2171, <https://doi.org/10.1002/2016JF003914>, 2016.
- 955 Brosens, L., Campforts, B., Robinet, J., Vanacker, V., Opfergelt, S., Ameijeiras-Mariño, Y., Minella, J. P. G., and
956 Govers, G.: Slope Gradient Controls Soil Thickness and Chemical Weathering in Subtropical Brazil:
957 Understanding Rates and Timescales of Regional Soilscape Evolution Through a Combination of Field Data
958 and Modeling, *J. Geophys. Res. Earth Surf.*, 125, 1, <https://doi.org/10.1029/2019JF005321>, 2020.
- 959 Carretier, S., Godd eris, Y., Delannoy, T., and Rouby, D.: Mean bedrock-to-saprolite conversion and erosion rates
960 during mountain growth and decline, *Geomorphology*, 209, 39–52,
961 <https://doi.org/10.1016/j.geomorph.2013.11.025>, 2014.
- 962 Cerqueira, R.: The Distribution of Didelphis in South America (Polyprotodontia, Didelphidae), *Journal of*
963 *Biogeography*, 12, 135, <https://doi.org/10.2307/2844837>, 1985.
- 964 Chen, M., Ma, L., Shao, M. a., Wei, X., Jia, Y., Sun, S., Zhang, Q., Li, T., Yang, X., and Gan, M.: Chinese zokor
965 (*Myospalax fontanierii*) excavating activities lessen runoff but facilitate soil erosion – A simulation
966 experiment, *CATENA*, 202, 105248, <https://doi.org/10.1016/j.catena.2021.105248>, 2021.
- 967 Choi, K., Arnhold, S., Huwe, B., and Reineking, B.: Daily Based Morgan–Morgan–Finney (DMMF) Model: A
968 Spatially Distributed Conceptual Soil Erosion Model to Simulate Complex Soil Surface Configurations,
969 *Water*, 9, 278, <https://doi.org/10.3390/w9040278>, 2017.
- 970 Cohen, S., Willgoose, G., Svoray, T., Hancock, G., and Sela, S.: The effects of sediment transport, weathering, and
971 aeolian mechanisms on soil evolution, *J. Geophys. Res. Earth Surf.*, 120, 260–274,
972 <https://doi.org/10.1002/2014JF003186>, 2015.
- 973 Cohen, S., Willgoose, G., and Hancock, G.: The mARM3D spatially distributed soil evolution model: Three-
974 dimensional model framework and analysis of hillslope and landform responses, *J. Geophys. Res.*, 115, 191,
975 <https://doi.org/10.1029/2009JF001536>, 2010.
- 976 Coombes, M. A.: Biogeomorphology: diverse, integrative and useful, *Earth Surf. Process. Landforms*, 41, 2296–
977 2300, <https://doi.org/10.1002/esp.4055>, 2016.
- 978 Corenblit, D., Corbara, B., and Steiger, J.: Biogeomorphological eco-evolutionary feedback between life and
979 geomorphology: a theoretical framework using fossorial mammals, *Die Naturwissenschaften*, 108, 55,
980 <https://doi.org/10.1007/s00114-021-01760-y>, 2021.
- 981 Debruyne, L. A.L. and Conacher, A. J.: The bioturbation activity of ants in agricultural and naturally vegetated
982 habitats in semiarid environments, *Soil Res.*, 32, 555, <https://doi.org/10.1071/SR9940555>, 1994.
- 983 Devia, G. K., Ganasri, B. P., and Dwarakish, G. S.: A Review on Hydrological Models, *Aquatic Procedia*, 4, 1001–
984 1007, <https://doi.org/10.1016/j.aqpro.2015.02.126>, 2015.
- 985 Durner, W., Iden, S. C., and Unold, G. von: The integral suspension pressure method (ISP) for precise particle-size
986 analysis by gravitational sedimentation, *Water Resour. Res.*, 53, 33–48, <https://doi.org/10.1002/2016WR019830>,
987 2017.
- 988 Eccard, J. A. and Herde, A.: Seasonal variation in the behaviour of a short-lived rodent, *BMC ecology*, 13, 43,
989 <https://doi.org/10.1186/1472-6785-13-43>, 2013.
- 990 Ferro, L. I. and Barquez, R. M.: Species Richness of Nonvolant Small Mammals Along Elevational Gradients in
991 Northwestern Argentina, *Biotropica*, 41, 759–767, <https://doi.org/10.1111/j.1744-7429.2009.00522.x>, 2009.
- 992 Foster, D. W.: BIOTURB: A FORTRAN program to simulate the effects of bioturbation on the vertical distribution
993 of sediment, *Computers & Geosciences*, 11, 39–54, [https://doi.org/10.1016/0098-3004\(85\)90037-8](https://doi.org/10.1016/0098-3004(85)90037-8), 1985.

- 994 François, F., Poggiale, J.-C., Durbec, J.-P., and Stora, G.: A New Approach for the Modelling of Sediment
995 Reworking Induced by a Macrobenthic Community, *Acta Biotheoretica*, 45, 295–319,
996 <https://doi.org/10.1023/A:1000636109604>, 1997.
- 997 Gabet, E. J.: Gopher bioturbation: field evidence for non-linear hillslope diffusion, *Earth Surf. Process. Landforms*,
998 25, 1419–1428, [https://doi.org/10.1002/1096-9837\(200012\)25:13<1419:AID-ESP148>3.0.CO;2-1](https://doi.org/10.1002/1096-9837(200012)25:13<1419:AID-ESP148>3.0.CO;2-1), 2000.
- 999 Gabet, E. J., Perron, J. T., and Johnson, D. L.: Biotic origin for Mima mounds supported by numerical modeling,
1000 *Geomorphology*, 206, 58–66, <https://doi.org/10.1016/j.geomorph.2013.09.018>, 2014.
- 1001 Gabet, E. J., Reichman, O. J., and Seabloom, E. W.: The Effects of Bioturbation on Soil Processes and Sediment
1002 Transport, *Annu. Rev. Earth Planet. Sci.*, 31, 249–273, <https://doi.org/10.1146/annurev.earth.31.100901.141314>,
1003 2003.
- 1004 Gray, H. J., Keen-Zebert, A., Furbish, D. J., Tucker, G. E., and Mahan, S. A.: Depth-dependent soil mixing persists
1005 across climate zones, *Proceedings of the National Academy of Sciences of the United States of America*, 117,
1006 8750–8756, <https://doi.org/10.1073/pnas.1914140117>, 2020.
- 1007 Grigusova, P., Larsen, A., Achilles, S., Brandl, R., del Río, C., Farwig, N., Kraus, D., Paulino, L., Plissock, P.,
1008 Übernicketel, K., and Bendix, J.: Higher sediment redistribution rates related to burrowing animals than
1009 previously assumed as revealed by time-of-flight-based monitoring, *Earth Surf. Dynam.*, 10, 1273–1301,
1010 <https://doi.org/10.5194/esurf-10-1273-2022>, 2022.
- 1011 Grigusova, P., Larsen, A., Achilles, S., Klug, A., Fischer, R., Kraus, D., Übernicketel, K., Paulino, L., Plissock, P.,
1012 Brandl, R., Farwig, N., and Bendix, J.: Area-Wide Prediction of Vertebrate and Invertebrate Hole Density and
1013 Depth across a Climate Gradient in Chile Based on UAV and Machine Learning, *Drones*, 5, 86,
1014 <https://doi.org/10.3390/drones5030086>, 2021.
- 1015 Hakonson, T. E.: The Effects of Pocket Gopher Burrowing on Water Balance and Erosion from Landfill Covers, *J.*
1016 *environ. qual.*, 28, 659–665, <https://doi.org/10.2134/jeq1999.00472425002800020033x>, 1999.
- 1017 Hall, K., Boelhouwers, J., and Driscoll, K.: Animals as Erosion Agents in the Alpine Zone: Some Data and
1018 Observations from Canada, Lesotho, and Tibet, *Arctic, Antarctic, and Alpine Research*, 31, 436–446,
1019 <https://doi.org/10.1080/15230430.1999.12003328>, 1999.
- 1020 Hancock, G. and Lowry, J.: Quantifying the influence of rainfall, vegetation and animals on soil erosion and
1021 hillslope connectivity in the monsoonal tropics of northern Australia, *Earth Surf. Process. Landforms*, 46,
1022 2110–2123, <https://doi.org/10.1002/esp.5147>, 2021.
- 1023 Hazelhoff, L., van Hoof, P., Imeson, A. C., and Kwaad, F. J. P. M.: The exposure of forest soil to erosion by
1024 earthworms, *Earth Surf. Process. Landforms*, 6, 235–250, <https://doi.org/10.1002/esp.3290060305>, 1981.
- 1025 Horn, B.K.P.: Hill shading and the reflectance map, *Proc. IEEE*, 69, 14–47,
1026 <https://doi.org/10.1109/PROC.1981.11918>, 1981.
- 1027 Imeson, A. C. and Kwaad, F. J. P. M.: Some Effects of Burrowing Animals on Slope Processes in the Luxembourg
1028 Ardennes, *Geografiska Annaler: Series A, Physical Geography*, 58, 317–328,
1029 <https://doi.org/10.1080/04353676.1976.11879941>, 1976.
- 1030 Istanbuluoglu, E.: Vegetation-modulated landscape evolution: Effects of vegetation on landscape processes,
1031 drainage density, and topography, *J. Geophys. Res.*, 110, 11, <https://doi.org/10.1029/2004JF000249>, 2005.
- 1032 Jimenez, J. E., Feinsinger, P., and Jaksi, F. M.: Spatiotemporal Patterns of an Irruption and Decline of Small
1033 Mammals in Northcentral Chile, *Journal of Mammalogy*, 73, 356–364, <https://doi.org/10.2307/1382070>, 1992.
- 1034 Jong, S. M. de, Paracchini, M. L., Bertolo, F., Folving, S., Megier, J., and Roo, A.P.J. de: Regional assessment of soil
1035 erosion using the distributed model SEMMED and remotely sensed data, *CATENA*, 37, 291–308,
1036 [https://doi.org/10.1016/S0341-8162\(99\)00038-7](https://doi.org/10.1016/S0341-8162(99)00038-7), 1999.

- 1037 Jumars, P. A., Nowell, A. R.M., and Self, R. F.L.: A simple model of flow —Sediment—Organism interaction,
1038 *Marine Geology*, 42, 155–172, [https://doi.org/10.1016/0025-3227\(81\)90162-6](https://doi.org/10.1016/0025-3227(81)90162-6), 1981.
- 1039 Kadko, D. and Heath, G. R.: Models of depth-dependent bioturbation at MANOP Site H in the eastern equatorial
1040 Pacific, *J. Geophys. Res.*, 89, 6567, <https://doi.org/10.1029/JC089iC04p06567>, 1984.
- 1041 Katzman, E. A., Zaytseva, E. A., Feoktistova, N. Y., Tovpinetz, N. N., Bogomolov, P. L., Potashnikova, E. V., and
1042 Surov, A. V.: Seasonal Changes in Burrowing of the Common Hamster (*Cricetus cricetus* L., 1758) (Rodentia:
1043 Cricetidae) in the City, *PJE*, 17, 251–258, <https://doi.org/10.18500/1684-7318-2018-3-251-258>, 2018.
- 1044 Kinlaw, A. and Grasmueck, M.: Evidence for and geomorphologic consequences of a reptilian ecosystem
1045 engineer: The burrowing cascade initiated by the Gopher Tortoise, *Geomorphology*, 157-158, 108–121,
1046 <https://doi.org/10.1016/j.geomorph.2011.06.030>, 2012.
- 1047 Kirols, H. S., Kevorkov, D., Uihlein, A., and Medraj, M.: The effect of initial surface roughness on water droplet
1048 erosion behaviour, *Wear*, 342-343, 198–209, <https://doi.org/10.1016/j.wear.2015.08.019>, 2015.
- 1049 Kraus, D., Brandl, R., Achilles, S., Bendix, J., Grigusova, P., Larsen, A., Plischoff, P., Übernickel, K., and Farwig, N.:
1050 Vegetation and vertebrate abundance as drivers of bioturbation patterns along a climate gradient, *PloS one*,
1051 17, e0264408, <https://doi.org/10.1371/journal.pone.0264408>, 2022.
- 1052 Kügler, M., Hoffmann, T. O., Beer, A. R., Übernickel, K., Ehlers, T. A., Scherler, D., and Eichel, J.: (LiDAR) 3D
1053 Point Clouds and Topographic Data from the Chilean Coastal Cordillera, 2022.
- 1054 La Croix, A. D., Gingras, M. K., Dashtgard, S. E., and Pemberton, S. G.: Computer modeling bioturbation: The
1055 creation of porous and permeable fluid-flow pathways, *Bulletin*, 96, 545–556,
1056 <https://doi.org/10.1306/07141111038>, 2012.
- 1057 Larsen, A., Nardin, W., Lageweg, W. I., and Bätz, N.: Biogeomorphology, quo vadis? On processes, time, and
1058 space in biogeomorphology, *Earth Surf. Process. Landforms*, 46, 12–23, <https://doi.org/10.1002/esp.5016>, 2021.
- 1059 Le Hir, P., Monbet, Y., and Orvain, F.: Sediment erodability in sediment transport modelling: Can we account for
1060 biota effects?, *Continental Shelf Research*, 27, 1116–1142, <https://doi.org/10.1016/j.csr.2005.11.016>, 2007.
- 1061 Lehnert, L. W., Thies, B., Trachte, K., Achilles, S., Osses, P., Baumann, K., Schmidt, J., Samolov, E., Jung, P.,
1062 Leinweber, P., Karsten, U., Büdel, B., and Bendix, J.: A Case Study on Fog/Low Stratus Occurrence at Las
1063 Lomitas, Atacama Desert (Chile) as a Water Source for Biological Soil Crusts, *Aerosol Air Qual. Res.*, 18, 254-
1064 26, <https://doi.org/10.4209/aaqr.2017.01.0021>, 2018.
- 1065 Li, G., Li, X., Li, J., Chen, W., Zhu, H., Zhao, J., and Hu, X.: Influences of Plateau Zokor Burrowing on Soil Erosion
1066 and Nutrient Loss in Alpine Meadows in the Yellow River Source Zone of West China, *Water*, 11, 2258,
1067 <https://doi.org/10.3390/w11112258>, 2019a.
- 1068 Li, T. C., Shao, M. A., Jia, Y. H., Jia, X. X., Huang, L. M., and Gan, M.: Small-scale observation on the effects of
1069 burrowing activities of ants on soil hydraulic processes, *Eur J Soil Sci*, 70, 236–244,
1070 <https://doi.org/10.1111/ejss.12748>, 2019b.
- 1071 Li, T., Shao, M. a., Jia, Y., Jia, X., and Huang, L.: Small-scale observation on the effects of the burrowing activities
1072 of mole crickets on soil erosion and hydrologic processes, *Agriculture, Ecosystems & Environment*, 261, 136–
1073 143, <https://doi.org/10.1016/j.agee.2018.04.010>, 2018.
- 1074 Li, Z. and Zhang, J.: Calculation of Field Manning’s Roughness Coefficient, *Agricultural Water Management*, 49,
1075 153–161, [https://doi.org/10.1016/S0378-3774\(00\)00139-6](https://doi.org/10.1016/S0378-3774(00)00139-6), 2001.
- 1076 Lilhare, R., Garg, V., and Nikam, B. R.: Application of GIS-Coupled Modified MMF Model to Estimate Sediment
1077 Yield on a Watershed Scale, *J. Hydrol. Eng.*, 20, 745, [https://doi.org/10.1061/\(ASCE\)HE.1943-5584.0001063](https://doi.org/10.1061/(ASCE)HE.1943-5584.0001063),
1078 2015.

- 1079 López-Vicente, M., Navas, A., and Machín, J.: Modelling soil detachment rates in rainfed agrosystems in the
1080 south-central Pyrenees, *Agricultural Water Management*, 95, 1079–1089,
1081 <https://doi.org/10.1016/j.agwat.2008.04.004>, 2008.
- 1082 Malizia, A. I.: Population dynamics of the fossorial rodent *Ctenomys talarum* (Rodentia: Octodontidae), *Journal*
1083 *of Zoology*, 244, 545–551, <https://doi.org/10.1111/j.1469-7998.1998.tb00059.x>, 1998.
- 1084 Meserve, P. L.: Trophic Relationships among Small Mammals in a Chilean Semiarid Thorn Scrub Community,
1085 *Journal of Mammalogy*, 62, 304–314, <https://doi.org/10.2307/1380707>, 1981.
- 1086 Meyer, H., Reudenbach, C., Hengl, T., Katurji, M., and Nauss, T.: Improving performance of spatio-temporal
1087 machine learning models using forward feature selection and target-oriented validation, *Environmental*
1088 *Modelling & Software*, 101, 1–9, <https://doi.org/10.1016/j.envsoft.2017.12.001>, 2018.
- 1089 Meysman, F. J. R., Boudreau, B. P., and Middelburg, J. J.: Relations between local, nonlocal, discrete and
1090 continuous models of bioturbation, *J Mar Res*, 61, 391–410, <https://doi.org/10.1357/002224003322201241>, 2003.
- 1091 Milstead, W. B., Meserve, P. L., Campanella, A., Previtali, M. A., Kelt, D. A., and Gutiérrez, J. R.: Spatial Ecology
1092 of Small Mammals in North-central Chile: Role of Precipitation and Refuges, *Journal of Mammalogy*, 88,
1093 1532–1538, <https://doi.org/10.1644/16-MAMM-A-407R.1>, 2007.
- 1094 Monteverde, M. J. and Piudo, L.: Activity Patterns of the Culpeo Fox (*Lycalopex Culpaeus Magellanica*) in a
1095 Non-Hunting Area of Northwestern Patagonia, Argentina, *Mammal Study*, 36, 119–125,
1096 <https://doi.org/10.3106/041.036.0301>, 2011.
- 1097 Morgan, R. P. C. and Duzant, J. H.: Modified MMF (Morgan–Morgan–Finney) model for evaluating effects of
1098 crops and vegetation cover on soil erosion, *Earth Surf. Process. Landforms*, 33, 90–106,
1099 <https://doi.org/10.1002/esp.1530>, 2008.
- 1100 Morgan, R. P. C., Quinton, J. N., Smith, R. E., Govers, G., Poesen, J. W. A., Auerswald, K., Chisci, G., Torri, D., and
1101 Styczen, M. E.: The European Soil Erosion Model (EUROSEM): a dynamic approach for predicting sediment
1102 transport from fields and small catchments, *Earth Surf. Process. Landforms*, 23, 527–544,
1103 [https://doi.org/10.1002/\(SICI\)1096-9837\(199806\)23:6<527:AID-ESP868>3.0.CO;2-5](https://doi.org/10.1002/(SICI)1096-9837(199806)23:6<527:AID-ESP868>3.0.CO;2-5), 1998.
- 1104 Morgan, R.P.C.: A simple approach to soil loss prediction: a revised Morgan–Morgan–Finney model, *CATENA*,
1105 44, 305–322, [https://doi.org/10.1016/S0341-8162\(00\)00171-5](https://doi.org/10.1016/S0341-8162(00)00171-5), 2001.
- 1106 Morgan, R.P.C., Morgan, D.D.V., and Finney, H. J.: A predictive model for the assessment of soil erosion risk,
1107 *Journal of Agricultural Engineering Research*, 30, 245–253, [https://doi.org/10.1016/S0021-8634\(84\)80025-6](https://doi.org/10.1016/S0021-8634(84)80025-6),
1108 1984.
- 1109 Nearing, M. A., Foster, G. R., Lane, L. J., and Finkner, S. C.: A Process-Based Soil Erosion Model for USDA-Water
1110 Erosion Prediction Project Technology, *Transactions of the ASAE*, 32, 1587–1593,
1111 <https://doi.org/10.13031/2013.31195>, 1989.
- 1112 Nkem, J. N., Lobry de Bruyn, L. A., Grant, C. D., and Hulugalle, N. R.: The impact of ant bioturbation and
1113 foraging activities on adjacent soil properties, *Pedobiologia*, 44, 609–621, [https://doi.org/10.1078/S0031-4056\(04\)70075-X](https://doi.org/10.1078/S0031-4056(04)70075-X), 2000.
- 1115 Oeser, R. A., Stroncik, N., Moskwa, L.-M., Bernhard, N., Schaller, M., Canessa, R., van den Brink, L., Köster, M.,
1116 Brucker, E., Stock, S., Fuentes, J. P., Godoy, R., Matus, F. J., Osés Pedraza, R., Osses McIntyre, P., Paulino, L.,
1117 Seguel, O., Bader, M. Y., Boy, J., Dippold, M. A., Ehlers, T. A., Kühn, P., Kuzyakov, Y., Leinweber, P.,
1118 Scholten, T., Spielvogel, S., Spohn, M., Übernickel, K., Tielbörger, K., Wagner, D., and Blanckenburg, F. von:
1119 Chemistry and microbiology of the Critical Zone along a steep climate and vegetation gradient in the Chilean
1120 Coastal Cordillera, *CATENA*, 170, 183–203, <https://doi.org/10.1016/j.catena.2018.06.002>, 2018.
- 1121 Orvain, F., Sauriau, P.-G., Bacher, C., and Prineau, M.: The influence of sediment cohesiveness on bioturbation
1122 effects due to *Hydrobia ulvae* on the initial erosion of intertidal sediments: A study combining flume and
1123 model approaches, *Journal of Sea Research*, 55, 54–73, <https://doi.org/10.1016/j.seares.2005.10.002>, 2006.

- 1124 Pelletier, J. D., Barron-Gafford, G. A., Breshears, D. D., Brooks, P. D., Chorover, J., Durcik, M., Harman, C. J.,
 1125 Huxman, T. E., Lohse, K. A., Lybrand, R., Meixner, T., McIntosh, J. C., Papuga, S. A., Rasmussen, C., Schaap,
 1126 M., Swetnam, T. L., and Troch, P. A.: Coevolution of nonlinear trends in vegetation, soils, and topography
 1127 with elevation and slope aspect: A case study in the sky islands of southern Arizona, *J. Geophys. Res. Earth*
 1128 *Surf.*, 118, 741–758, <https://doi.org/10.1002/jgrf.20046>, 2013.
- 1129 Penman, H.: Natural evaporation from open water, bare soil and grass, *Proceedings of the Royal Society of*
 1130 *London. Series A, Mathematical and physical sciences*, 193, 120–145, <https://doi.org/10.1098/rspa.1948.0037>,
 1131 1948.
- 1132 Pollacco, J. A. P.: A generally applicable pedotransfer function that estimates field capacity and permanent
 1133 wilting point from soil texture and bulk density, *Can. J. Soil. Sci.*, 88, 761–774,
 1134 <https://doi.org/10.4141/CJSS07120>, 2008.
- 1135 Qin, Y., Yi, S., Ding, Y., Qin, Y., Zhang, W., Sun, Y., Hou, X., Yu, H., Meng, B., Zhang, H., Chen, J., and Wang, Z.:
 1136 Effects of plateau pikas' foraging and burrowing activities on vegetation biomass and soil organic carbon of
 1137 alpine grasslands, *Plant Soil*, 458, 201–216, <https://doi.org/10.1007/s11104-020-04489-1>, 2021.
- 1138 Reichman, O. J. and Seabloom, E. W.: The role of pocket gophers as subterranean ecosystem engineers, *Trends in*
 1139 *Ecology & Evolution*, 17, 44–49, [https://doi.org/10.1016/S0169-5347\(01\)02329-1](https://doi.org/10.1016/S0169-5347(01)02329-1), 2002.
- 1140 Renard, K., Foster, G., Weesies, G., and Porter, J.: RUSLE: The Revised Universal Soil Loss Equation, *Journal of*
 1141 *Soil Water Conservation*, 30–33, 1991.
- 1142 Ridd, P. V.: Flow Through Animal Burrows in Mangrove Creeks, *Estuarine, Coastal and Shelf Science*, 43, 617–
 1143 625, <https://doi.org/10.1006/ecss.1996.0091>, 1996.
- 1144 Rodríguez-Caballero, E., Cantón, Y., Chamizo, S., Afana, A., and Solé-Benet, A.: Effects of biological soil crusts on
 1145 surface roughness and implications for runoff and erosion, *Geomorphology*, 145–146, 81–89,
 1146 <https://doi.org/10.1016/j.geomorph.2011.12.042>, 2012.
- 1147 Román-Sánchez, A., Reimann, T., Wallinga, J., and Vanwalleghem, T.: Bioturbation and erosion rates along the
 1148 soil-hillslope conveyor belt, part 1: Insights from single-grain feldspar luminescence, *Earth Surf. Process.*
 1149 *Landforms*, 44, 2051–2065, <https://doi.org/10.1002/esp.4628>, 2019.
- 1150 ROO, A. P. J. de, WESSELING, C. G., and RITSEMA, C. J.: LISEM: A SINGLE-EVENT PHYSICALLY BASED
 1151 HYDROLOGICAL AND SOIL EROSION MODEL FOR DRAINAGE BASINS. I: THEORY, INPUT AND
 1152 OUTPUT, *Hydrol. Process.*, 10, 1107–1117, [https://doi.org/10.1002/\(SICI\)1099-1085\(199608\)10:8<1107:AID-
 1153 HYP415>3.0.CO;2-4](https://doi.org/10.1002/(SICI)1099-1085(199608)10:8<1107:AID-HYP415>3.0.CO;2-4), 1996.
- 1154 Rutin, J.: The burrowing activity of scorpions (*Scorpio maurus palmatus*) and their potential contribution to the
 1155 erosion of Hamra soils in Karkur, central Israel, *Geomorphology*, 15, 159–168, [https://doi.org/10.1016/0169-
 1156 555X\(95\)00120-T](https://doi.org/10.1016/0169-555X(95)00120-T), 1996.
- 1157 Sanford, L. P.: Modeling a dynamically varying mixed sediment bed with erosion, deposition, bioturbation,
 1158 consolidation, and armoring, *Computers & Geosciences*, 34, 1263–1283,
 1159 <https://doi.org/10.1016/j.cageo.2008.02.011>, 2008.
- 1160 Schiffers, K., Teal, L. R., Travis, J. M. J., and Solan, M.: An open source simulation model for soil and sediment
 1161 bioturbation, *PloS one*, 6, e28028, <https://doi.org/10.1371/journal.pone.0028028>, 2011.
- 1162 Shannon, C. E.: A Mathematical Theory of Communication, *Bell System Technical Journal*, 27, 379–423,
 1163 <https://doi.org/10.1002/j.1538-7305.1948.tb01338.x>, 1948.
- 1164 Shull, D. H.: Transition-matrix model of bioturbation and radionuclide diagenesis, *Limnol. Oceanogr.*, 46, 905–
 1165 916, <https://doi.org/10.4319/lo.2001.46.4.0905>, 2001.
- 1166 Simonetti, J. A.: Microhabitat Use by Small Mammals in Central Chile, *Oikos*, 56, 309,
 1167 <https://doi.org/10.2307/3565615>, 1989.

- 1168 Soetaert, K., Herman, P. M. J., Middelburg, J. J., Heip, C., deStigter, H. S., van Weering, T. C. E., Epping, E., and
 1169 Helder, W.: Modeling ^{210}Pb -derived mixing activity in ocean margin sediments: Diffusive versus nonlocal
 1170 mixing, *J Mar Res*, 54, 1207–1227, <https://doi.org/10.1357/0022240963213808>, 1996.
- 1171 Taylor, A. R., Lenoir, L., Vegerfors, B., and Persson, T.: Ant and Earthworm Bioturbation in Cold-Temperate
 1172 Ecosystems, *Ecosystems*, 22, 981–994, <https://doi.org/10.1007/s10021-018-0317-2>, 2019.
- 1173 Temme, A. J.A.M. and Vanwallegem, T.: LORICA – A new model for linking landscape and soil profile
 1174 evolution: Development and sensitivity analysis, *Computers & Geosciences*, 90, 131–143,
 1175 <https://doi.org/10.1016/j.cageo.2015.08.004>, 2016.
- 1176 Tews, J., Brose, U., Grimm, V., Tielbörger, K., Wichmann, M. C., Schwager, M., and Jeltsch, F.: Animal species
 1177 diversity driven by habitat heterogeneity/diversity: the importance of keystone structures, *Journal of*
 1178 *Biogeography*, 31, 79–92, <https://doi.org/10.1046/j.0305-0270.2003.00994.x>, 2004.
- 1179 Tomasella, J., Hodnett, M. G., and Rossato, L.: Pedotransfer Functions for the Estimation of Soil Water Retention
 1180 in Brazilian Soils, *Soil Sci. Soc. Am. J.*, 64, 327–338, <https://doi.org/10.2136/sssaj2000.641327x>, 2000.
- 1181 Trauth, M. H.: TURBO: a dynamic-probabilistic simulation to study the effects of bioturbation on
 1182 paleoceanographic time series, *Computers & Geosciences*, 24, 433–441, [https://doi.org/10.1016/S0098-3004\(98\)00019-3](https://doi.org/10.1016/S0098-3004(98)00019-3), 1998.
- 1184 Tucker, G. E. and Hancock, G. R.: Modelling landscape evolution, *Earth Surf. Process. Landforms*, 35, 28–50,
 1185 <https://doi.org/10.1002/esp.1952>, 2010.
- 1186 Übernichel, K., Pizarro-Araya, J., Bhagavathula, S., Paulino, L., and Ehlers, T. A.: Reviews and syntheses:
 1187 Composition and characteristics of burrowing animals along a climate and ecological gradient, Chile,
 1188 *Biogeosciences*, 18, 5573–5594, <https://doi.org/10.5194/bg-18-5573-2021>, 2021a.
- 1189 Übernichel, K., Ehlers, T. A., Paulino, L., and Fuentes Espoz, J.-P.: Time series of meteorological stations on an
 1190 elevational gradient in National Park La Campana, Chile, 2021b.
- 1191 Vanwallegem, T., Stockmann, U., Minasny, B., and McBratney, A. B.: A quantitative model for integrating
 1192 landscape evolution and soil formation, *J. Geophys. Res. Earth Surf.*, 118, 331–347,
 1193 <https://doi.org/10.1029/2011JF002296>, 2013.
- 1194 Vieira, D.C.S., Prats, S. A., Nunes, J. P., Shakesby, R. A., Coelho, C.O.A., and Keizer, J. J.: Modelling runoff and
 1195 erosion, and their mitigation, in burned Portuguese forest using the revised Morgan–Morgan–Finney model,
 1196 *Forest Ecology and Management*, 314, 150–165, <https://doi.org/10.1016/j.foreco.2013.12.006>, 2014.
- 1197 Vigiak, O., Okoba, B. O., Sterk, G., and Groenenberg, S.: Modelling catchment-scale erosion patterns in the East
 1198 African Highlands, *Earth Surf. Process. Landforms*, 30, 183–196, <https://doi.org/10.1002/esp.1174>, 2005.
- 1199 Voiculescu, M., Ianăș, A.-N., and Germain, D.: Exploring the impact of snow vole (*Chionomys nivalis*) burrowing
 1200 activity in the Făgăraș Mountains, Southern Carpathians (Romania): Geomorphic characteristics and
 1201 sediment budget, *CATENA*, 181, 104070, <https://doi.org/10.1016/j.catena.2019.05.016>, 2019.
- 1202 Wang, B., Zheng, F., Römken, M. J.M., and Darboux, F.: Soil erodibility for water erosion: A perspective and
 1203 Chinese experiences, *Geomorphology*, 187, 1–10, <https://doi.org/10.1016/j.geomorph.2013.01.018>, 2013.
- 1204 Wei, X., Li, S., Yang, P., and Cheng, H.: Soil erosion and vegetation succession in alpine Kobresia steppe meadow
 1205 caused by plateau pika—A case study of Nagqu County, Tibet, *Chin. Geograph.Sc.*, 17, 75–81,
 1206 <https://doi.org/10.1007/s11769-007-0075-0>, 2007.
- 1207 Welivitiya, W. D. D. P., Willgoose, G. R., and Hancock, G. R.: A coupled soilscape–landform evolution model:
 1208 model formulation and initial results, *Earth Surf. Dynam.*, 7, 591–607, <https://doi.org/10.5194/esurf-7-591-2019>,
 1209 2019.

- 1210 Wheatcroft, R. A., Jumars, P. A., Smith, C. R., and Nowell, A. R. M.: A mechanistic view of the particulate
1211 biodiffusion coefficient: Step lengths, rest periods and transport directions, *J Mar Res*, 48, 177–207,
1212 <https://doi.org/10.1357/002224090784984560>, 1990.
- 1213 Whitesides, C. J. and Butler, D. R.: Bioturbation by gophers and marmots and its effects on conifer germination,
1214 *Earth Surf. Process. Landforms*, 41, 2269–2281, <https://doi.org/10.1002/esp.4046>, 2016.
- 1215 Wilkinson, M. T., Richards, P. J., and Humphreys, G. S.: Breaking ground: Pedological, geological, and ecological
1216 implications of soil bioturbation, *Earth-Science Reviews*, 97, 257–272,
1217 <https://doi.org/10.1016/j.earscirev.2009.09.005>, 2009.
- 1218 Williams, J. R. (Ed.): Sediment-yield prediction with Universal Equation using runoff energy factor. In Present
1219 and prospective technology for predicting sediment yield and sources: Proceedings of the Sediment-Yield
1220 Workshop, ARS-S-40, United States Department of Agriculture (USDA), New Orleans, USA, 1975.
- 1221 Wilson, M. F. J., O'Connell, B., Brown, C., Guinan, J. C., and Grehan, A. J.: Multiscale Terrain Analysis of
1222 Multibeam Bathymetry Data for Habitat Mapping on the Continental Slope, *Marine Geodesy*, 30, 3–35,
1223 <https://doi.org/10.1080/01490410701295962>, 2007.
- 1224 Wischmeier, W. and Smith, D. D.: Predicting rainfall erosion losses - A guide to conservation planning,
1225 *Agriculture Handbook*, 1–58, 1978.
- 1226 Wood, S. N.: Generalized Additive Models, Chapman and Hall/CRC, 2006.
- 1227 Wösten, J.H.M. (Ed.): Soil Quality for Crop Production and Ecosystem Health, *Developments in Soil Science*,
1228 Elsevier, 1997.
- 1229 Wu, C., Wu, H., Liu, D., Han, G., Zhao, P., and Kang, Y.: Crab bioturbation significantly alters sediment microbial
1230 composition and function in an intertidal marsh, *Estuarine, Coastal and Shelf Science*, 249, 107116,
1231 <https://doi.org/10.1016/j.ecss.2020.107116>, 2021.
- 1232 Yair, A.: Short and long term effects of bioturbation on soil erosion, water resources and soil development in an
1233 arid environment, *Geomorphology*, 13, 87–99, [https://doi.org/10.1016/0169-555X\(95\)00025-Z](https://doi.org/10.1016/0169-555X(95)00025-Z), 1995.
- 1234 Yoo, K. and Mudd, S. M.: Toward process-based modeling of geochemical soil formation across diverse
1235 landforms: A new mathematical framework, *Geoderma*, 146, 248–260,
1236 <https://doi.org/10.1016/j.geoderma.2008.05.029>, 2008.
- 1237 Yoo, K., Amundson, R., Heimsath, A. M., and Dietrich, W. E.: Process-based model linking pocket gopher
1238 (*Thomomys bottae*) activity to sediment transport and soil thickness, *J. Geophys. Res.*, 33, 917,
1239 <https://doi.org/10.1130/G21831.1>, 2005.
- 1240 Yu, C., Zhang, J., Pang, X. P., Wang, Q., Zhou, Y. P., and Guo, Z. G.: Soil disturbance and disturbance intensity:
1241 Response of soil nutrient concentrations of alpine meadow to plateau pika bioturbation in the Qinghai-
1242 Tibetan Plateau, China, *Geoderma*, 307, 98–106, <https://doi.org/10.1016/j.geoderma.2017.07.041>, 2017.
- 1243 Zevenbergen, L. W. and Thorne, C. R.: Quantitative analysis of land surface topography, *Earth Surf. Process.*
1244 *Landforms*, 12, 47–56, <https://doi.org/10.1002/esp.3290120107>, 1987.
- 1245 Zhang, Q., Li, J., Hu, G., and Zhang, Z.: Bioturbation potential of a macrofaunal community in Bohai Bay,
1246 northern China, *Marine pollution bulletin*, 140, 281–286, <https://doi.org/10.1016/j.marpolbul.2019.01.063>, 2019.
- 1247 Zhang, S., Fang, X., Zhang, J., Yin, F., Zhang, H., Wu, L., and Kitazawa, D.: The Effect of Bioturbation Activity of
1248 the Ark Clam *Scapharca subcrenata* on the Fluxes of Nutrient Exchange at the Sediment-Water Interface, *J.*
1249 *Ocean Univ. China*, 19, 232–240, <https://doi.org/10.1007/s11802-020-4112-2>, 2020.
- 1250